Fairing of planar curves to Euler's elasticae and log-aesthetic curves

グライフ, ズリタ, セバスティアン, エリアス

Dissertation for the Degree of Doctor of Philosophy

Fairing of planar curves to Euler's elasticae and log-aesthetic curves

Graduate School of Mathematics
Kyushu University

Sebastián Elías Graiff Zurita

Supervisor : Professor Kenji Kajiwara
Submission date : July 21, 2022

Acknowledgments

To MEXT, for providing the grant that has allowed me to study at Kyushu University; and to the CREST-ED3GE funding, for financially supporting this research.

To the CREST-ED3GE team members. Particularly, to my supervisor Prof. Kenji Kajiwara, who has helped all along the way with this work; and to Prof. Kenjiro T. Miura and Prof. Toshitomo Suzuki, who have helped with the applications for this work.

To my family, for their continued support from close by and at a distance.

To my friends from all around the world have always been my best resource of creativeness, motivation, and enjoyment.

Contents

Chapter 1

Introduction

Historically, the term fairing refers to a structure whose function is to improve the aerodynamics of a particular object. For example, a fairing helps reduce the drag of an airplane or boat. In this regard, to fair a given design is part of the process of streamlining. This concept was then translated to industrial design and architecture, and its meaning has widened to include smooth shapes that help structures fit more *naturally* in their environment. In this particular work, we investigate two families of curves that are closely related to the industry and to natural processes: The Euler's elasticae and the log-aesthetic curves.

The problem of the *elastica* is that of finding the shape that a thin strip of elastic material acquired when it is bent. The most complete mathematical solution is attributed to Euler, hence the term Euler's elastica. It is interesting to know that the elastica serves as a mathematical model of the mechanical spline, used for shipbuilding and similar applications, and it directly inspired the modern theory of mathematical splines [28], which are widely used in computer-aided design and computer graphics. From a mathematical point of view, the Euler's elastica (or elastic curve) is a class of planar curves characterized as the solutions to the variational problem of minimizing the elastic energy under certain boundary conditions. It has been regarded as one of the most important classes of planar curves because it is endowed with rich mathematical structure: exact solutions, integrability, geometry of elliptic curves, and so on [31, 43]. D. Brander et al. [6] have proposed an algorithm to fair (to approximate) a given planar curve segment to an Euler's elastica, motivated mainly by the development of the robotic hot-blade cutting technology. In this thesis, motivated by the problem, in architecture, to characterize the profile keylines of Japanese handmade pantiles, where the curve data is obtained in the form of discrete point data, we aim to construct a fairing method of discrete planar curves by utilizing the integrable discrete analogue of the Euler's elastica proposed by A. I. Bobenko and Y. B. Suris [5].

The log-aesthetic curves (LAC) constitute a class of planar spirals that includes the logarithmic spiral, the Nielsen's spiral, the Cornu spiral, and the circle involute, among others. This family is defined to best represent the properties observed by T. Harada et al. [15], who set up an experiment to analyze aesthetically pleasing curves from the viewpoint of the observer. Their main result may be described as follows: the curves that car designers regard as aesthetically pleasing have the common property that the frequency histogram of the radius of curvature follows a piece-wise linear relation in a log-log scale. An analytic formulation of the LAC was provided in [36, 50], which promoted theoretical and practical studies of LAC towards their use in computer-aided geometric design as indicated by Levien and Séquin [29]. Several works have been written regarding the implementation and construction of LAC with fixed boundary conditions, see for example [10, 11, 51]. Furthermore, extensions to surfaces have also been considered with an emphasis on providing practical tools for industrial design, see [35]. From a different point of view, LAC have been characterized as curves that are obtained via a variational principle in the framework of similarity geometry, moreover, they can also be seen as invariant curves under the integrable flow on plane curves which is governed by the Burgers equation [23]. This fact was also shown to be useful at providing an integrable discretization of the LAC that preserves the underlying geometric structure [20]. All these previous works contributed to constructing methods that generate a desirable shape with given fixed conditions.

The goal of this thesis is to provide tools, founded on geometric properties, to be used in reverse engineering applications. In Chapter 2, we review the basic concepts of planar curves and discrete planar curves. In Chapter 3, we focus our attention to the Euler's elastica. We review, in Sections 3.1 and 3.2, the properties and results of the continuous and discrete Euler's elastica, respectively. In each instance, we show that all the discrete objects possess analogue properties than their continuous counterpart. In Section 3.3, we construct a method to fair a given discrete planar curve by using the integrable discrete analogue of Euler's elastica. In Chapter 4, in analogy to the previous chapter, we focus our attention to the LAC. In Section 4.1, we review some basic definitions and present a result showing that a general LAC segment can be uniquely identified by seven parameters. We use this result in Section 4.2 to construct an algorithmic method, assuming discrete input data, to approximate a given planar curve. Finally, in Chapter 5 we use our findings in two concrete applications. In Section 5.1, we characterize the profile keylines of Japanese handmade pantiles by the integrable discrete analogue of the Euler's elasticae and in Section 5.2 we characterize some simple profile lines of a car's roof by the LAC.

Chapter 2

Preliminaries

2.1 Planar curves

Let us start with some basic definitions of planar curves, in part to introduce the notation that we are going to use in this thesis. We use the convention that a point $P \in \mathbb{R}^2$ is expressed as a column vector, i.e.,

$$P = \begin{pmatrix} x \\ y \end{pmatrix} = {}^{\mathrm{t}}(x, y) \in \mathbb{R}^2. \tag{2.1}$$

We denote by R_φ to the counterclockwise rotation matrix of angle φ,

$$\mathrm{R}_\varphi = \begin{pmatrix} \cos\varphi & -\sin\varphi \\ \sin\varphi & \cos\varphi \end{pmatrix}. \tag{2.2}$$

Regarding the functions, the first, second, etc., derivative of any given function f will be denoted as $f'(t)$, $f''(t)$, etc., respectively. For the curves, we focus our attention only on a particular kind of planar curves, those which are *regular* and *smooth*, so we simply refer to them as planar curves. The notion of *smoothness* that we consider is that all orders of derivatives exist and are continuous. A more comprehensive introduction can be found in any introductory book on differential geometry of curves and surfaces (see, for example, [1, 7]).

Definition 2.1 — A *(regular and smooth) planar curve* is a function $\gamma : [t_0, t_1] \to \mathbb{R}^2$ defined over the interval $[t_0, t_1] \subset \mathbb{R}$ such that

(1) there exists a smooth function $\Gamma : I \to \mathbb{R}^2$ defined over an open set $I \supset [t_0, t_1]$ which extends the function γ, and

(2) its first derivative satisfies that $\|\gamma'(t)\| > 0$, $t \in [t_0, t_1]$.

Let $\gamma : [t_0, t_1] \to \mathbb{R}^2$ be a planar curve. Then, the **arc length** function is defined as

$$s(t) := \int_{t_0}^{t} \|\gamma'(t)\| \, \mathrm{d}t, \qquad t \in [t_0, t_1], \tag{2.3}$$

and the **total length** of γ as

$$L \equiv L[\gamma] := \int_{t_0}^{t_1} \|\gamma'(t)\| \, \mathrm{d}t. \tag{2.4}$$

The **tangent** and **normal** vectors are defined as

$$T(t) := \frac{\gamma'(t)}{\|\gamma'(t)\|}, \qquad t \in [t_0, t_1], \tag{2.5}$$

and

$$N(t) := \mathrm{R}_{\pi/2} \, T(t), \qquad t \in [t_0, t_1], \tag{2.6}$$

respectively, where $\mathrm{R}_{\pi/2}$ is a $\pi/2$ counterclockwise rotation matrix. Furthermore, the tangent and normal vectors, being unit vectors, are parameterized by the **turning angle** function $\psi : [t_0, t_1] \to \mathbb{R}$, such that

$$T(t) = \begin{pmatrix} \cos\psi(t) \\ \sin\psi(t) \end{pmatrix}, \qquad N(t) = \begin{pmatrix} -\sin\psi(t) \\ \cos\psi(t) \end{pmatrix}. \tag{2.7}$$

The (signed) **curvature** $\kappa : [t_0, t_1] \to \mathbb{R}$ is defined in such a way that it satisfies

$$T'(t) = s'(t)\kappa(t)N(t), \qquad t \in [t_0, t_1]. \tag{2.8}$$

The (signed) **radius of curvature** $\rho(t)$ at a point $t \in [t_0, t_1]$ is defined as the radius of the osculating circle of $\gamma(t)$ at the point t, i.e.,

$$\rho(t) := \frac{1}{\psi'(t)} s'(t). \tag{2.9}$$

At each point $\gamma(t)$, the orthonormal basis $\{T(t), N(t)\}$ of $\mathbb{R}^2$ helps describe the local properties of the curve. This basis is called the **Frenet frame** and it is identified with elements of the special orthogonal group by

$$\Phi(t) := [T(t), N(t)] \in \mathrm{SO}(2), \qquad t \in [t_0, t_1]. \tag{2.10}$$

Finally, from (2.6) and (2.8), it can be seen that the equation of motion of the Frenet frame, which moves along the curve, satisfies that

$$\Phi'(t) = \Phi(t)L(t), \qquad L(t) = \begin{pmatrix} 0 & -s'(t)\kappa(t) \\ s'(t)\kappa(t) & 0 \end{pmatrix}, \tag{2.11}$$

which is called the **Frenet formula**.

Remark 2.2 — Consider the tangent vector parameterized by the turning angle, as in (2.7). Then, it is easy to see that

$$T'(t) = \psi'(t)N(t). \tag{2.12}$$

Thus, by comparing (2.12) with (2.8), we obtain an expression for the curvature in terms of the turning angle, as

$$\kappa(t) = \frac{1}{s'(t)}\psi'(t), \tag{2.13}$$

which provides a simple relationship between the radius of curvature and the curvature,

$$\rho(t) = \frac{1}{\kappa(t)}. \tag{2.14}$$

Note that the arc length function (2.3) of a (regular) curve $\gamma(t)$, $t \in [t_0, t_1]$, is a smooth function with nowhere vanishing first derivative; hence, it is a strictly monotonic smooth bijection with its image $s([t_0, t_1]) = [0, L] \subset \mathbb{R}$. With this in mind, we can always find a reparameterization $\bar{\gamma}(\bar{s}) = (\gamma \circ s^{-1})(\bar{s})$, $\bar{s} \in [0, L]$, such that the parameter $\bar{s}$ represents the partial length of the curve. This parameter is called the **arc length** parameter and, when there is no confusion with its corresponding function, will be denoted as s, as well.

Definition 2.3 — A curve $\gamma : [s_0, s_1] \to \mathbb{R}^2$ is *parameterized by arc length* if and only if $\|\gamma'(s)\| = 1$ for all $s \in [s_0, s_1]$.

Remark 2.4 — Note that the total length of an arc length parameterized curve $\gamma(s)$, $s \in [s_0, s_1]$, is $L = s_1 - s_0$, the tangent vector is $T(s) = \gamma'(s)$, the curvature satisfies $T'(s) = \kappa(s)N(s)$, and can be computed as $\kappa(s) = \psi'(s)$.

Theorem 2.5 (Fundamental Theorem of Planar Curves) **—** *Given a function $\kappa : [s_0, s_1] \to \mathbb{R}$, there exists a curve $\gamma : [s_0, s_1] \to \mathbb{R}^2$ parameterized by arc length which has κ as its curvature function. Furthermore, this curve is uniquely determined up to rigid transformations of the plane.*

Proof. From the expression $\kappa(s) = \psi'(s)$, for the curvature of an arc length parameterized curve, we find that

$$\psi_i(s) = \int_{s_0}^{s} \kappa(\bar{s})\, \mathrm{d}\bar{s} + \psi_i, \qquad s \in [s_0, s_1] \tag{2.15}$$

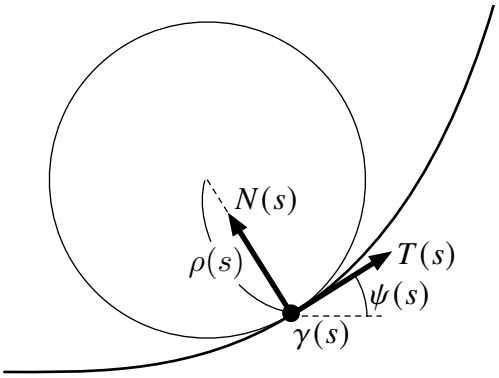

Figure 2.1: Representation of a planar curve and its relation to the Frenet frame, the turning angle, and the radius of curvature.

for some $\psi_i \in \mathbb{R}$. Then, from $T(s) = \gamma'(s)$ we obtain

$$\gamma_i(s) := \int_{s_0}^{s} \begin{pmatrix} \cos\psi_i(\bar{s}) \\ \sin\psi_i(\bar{s}) \end{pmatrix} \mathrm{d}\bar{s} + \begin{pmatrix} x_i \\ y_i \end{pmatrix}, \qquad s \in [s_0, s_1], \tag{2.16}$$

for some ${}^{\mathrm{t}}(x_i, y_i) \in \mathbb{R}^2$. By construction, γ_i is an arc length parameterized curve with curvature κ. Moreover, (2.16) is the general solution for such curves. For the second part, assume γ_1 and γ_2 are two arc length parameterized curves with curvature κ, described by (2.16) with constants $\{\psi_1, x_1, y_1\}$ and $\{\psi_2, x_2, y_2\}$, respectively. Then, it is easy to see that

$$\gamma_2 = \begin{pmatrix} \cos(\psi_2 - \psi_1) & -\sin(\psi_2 - \psi_1) \\ \sin(\psi_2 - \psi_1) & \cos(\psi_2 - \psi_1) \end{pmatrix} \left(\gamma_1 - \begin{pmatrix} x_1 \\ y_1 \end{pmatrix} \right) + \begin{pmatrix} x_2 \\ y_2 \end{pmatrix}, \tag{2.17}$$

which shows that γ_1 and γ_2 differ only by rigid transformations of the plane. □

Corollary 2.6 — *Given a function $\psi : [s_0, s_1] \to \mathbb{R}$, there exists an arc length parameterized curve $\gamma : [s_0, s_1] \to \mathbb{R}^2$ which has ψ as its turning angle function. Furthermore, this curve is uniquely determined up to translations of the plane.*

The last two results are telling us that any curve can be completely characterized in terms of its curvature or turning angle function, disregarding any rigid motion of the plane. The equations of the curvature or the turning angle in terms of the arc length parameter are consider to be *intrinsic equations*, in the sense that they represent qualities of the curve that do not change from system to system. In the literature, equation relating the curvature and arc length are known as Cesáro equations, and equations relating the turning angle and the arc length are known as Whewell equations [49].

Example 2.7 (Euler's elastica) — Consider $\psi(s)$, $s \in [s_0, s_1]$, such that

$$\psi'' + \mu \sin\psi = 0, \tag{2.18}$$

for some $\mu > 0$. This differential equation can be solved by exploiting the properties of the Jacobi elliptic functions. It is easy to check that

$$\sin\frac{\psi(s)}{2} = \operatorname{sn}\left(k^{-1}\sqrt{\mu}s; k\right), \qquad \cos\frac{\psi(s)}{2} = \operatorname{cn}\left(k^{-1}\sqrt{\mu}s; k\right), \tag{2.19}$$

for some $k > 0$, is an implicit solution of (2.18). In particular, we use the following three properties for the functions $\operatorname{sn}(u;k)$, $\operatorname{cn}(u;k)$, and $\operatorname{dn}(u;k)$, of modulus k,

$$(\operatorname{sn}(u;k))^2 + (\operatorname{cn}(u;k))^2 = 1, \tag{2.20}$$

$$\frac{\mathrm{d}}{\mathrm{d}u}\operatorname{sn}(u;k) = \operatorname{cn}(u;k)\operatorname{dn}(u;k), \tag{2.21}$$

$$\frac{\mathrm{d}}{\mathrm{d}u}\operatorname{dn}(u;k) = -k^2\operatorname{sn}(u;k)\operatorname{cn}(u;k). \tag{2.22}$$

From (2.20) and (2.21) we get

$$\psi'(s) = 2k^{-1}\sqrt{\mu}\operatorname{dn}\left(k^{-1}\sqrt{\mu}s; k\right). \tag{2.23}$$

Then, we take the derivative of (2.23) and use (2.22) to prove that (2.18) holds. Furthermore, (2.23) gives the expression for the curvature, which is computed as $\kappa(s) = \psi'(s)$.

2.2 Discrete planar curves

For discrete systems, there is no general framework accepted as canonical. In fact, depending on the uses, different definitions coexist and are welcome. This is more noticeable for derived quantities, for example the discrete tangent, discrete curvature, discrete Frenet frame, and so on. In our case, we follow the notion of discrete curves provided in [3, 18].

Definition 2.8 — A *discrete (regular) planar curve* of size $N \in \mathbb{N}$ is a map $\gamma : [0, N-1] \cap \mathbb{N} \to \mathbb{R}^2$ defined over the integers, identified by $\gamma(n) \equiv \gamma_n$, that satisfies

$$\det\left(\gamma_{n+1} - \gamma_n, \gamma_n - \gamma_{n-1}\right) \neq 0, \qquad n = 1, \ldots, N-2, \tag{2.24}$$

which means that there are no three consecutive points in the plane that are collinear. Moreover, if

$$\|\gamma_{n+1} - \gamma_n\| = \|\gamma_n - \gamma_{n-1}\|, \qquad n = 1, \ldots, N-2, \tag{2.25}$$

the discrete planar curve is referred to as *parameterized by arc length*, with step size h, defined by

$$h := \|\gamma_1 - \gamma_0\| \in \mathbb{R} - \{0\}. \tag{2.26}$$

Remark 2.9 — In what follows, and for the remaining of this thesis, unless explicitly mentioned, let us assume that all the discrete planar curves are parameterized by arc length. Furthermore, when it is understood from the context, we omit the expression *discrete* before the name of each discrete object.

Let γ_n, $n = 0, \ldots, N-1$, be a discrete planar curve with step size h. The **(discrete) total length** is defined as

$$L := \sum_{n=0}^{N-2} \|\gamma_{n+1} - \gamma_n\| = (N-1)h. \tag{2.27}$$

The **(discrete) tangent** and **(discrete) normal** vectors are defined as

$$T_n := \frac{\gamma_{n+1} - \gamma_n}{\|\gamma_{n+1} - \gamma_n\|}, \qquad n = 0, \ldots, N-2, \tag{2.28}$$

and

$$N_n := \mathrm{R}_{\pi/2}\, T_n, \qquad n = 0, \ldots, N-2, \tag{2.29}$$

respectively, where $\mathrm{R}_{\pi/2}$ is the $\pi/2$ counterclockwise rotation matrix. Likewise the smooth case, we parameterize the tangent and normal vectors by the **(discrete) turning angle** ψ_n, such that

$$T_n = \begin{pmatrix} \cos\psi_n \\ \sin\psi_n \end{pmatrix}, \qquad N_n = \begin{pmatrix} -\sin\psi_n \\ \cos\psi_n \end{pmatrix}, \quad n = 0, \ldots, N-2. \tag{2.30}$$

Furthermore, we define the **deflection angle** by

$$K_n := \psi_n - \psi_{n-1} \in (-\pi, \pi), \qquad n = 1, \ldots, N-2. \tag{2.31}$$

Analogously to (2.9) in the smooth case, the **(discrete) radius of curvature** is defined as the radius of the circle osculating at the middle points of two consecutive segments of the discrete curve, i.e.,

$$\rho_n := \frac{h}{2\tan\left(\frac{K_n}{2}\right)}. \tag{2.32}$$

Moreover, along the same lines as the smooth case, the **(discrete) curvature** is defined as the inverse of the radius of curvature,

$$\kappa_n := \frac{2}{h}\tan\left(\frac{K_n}{2}\right). \tag{2.33}$$

The **(discrete) Frenet frame** is defined by

$$\Phi_n = [T_n, N_n] \in \mathrm{SO}(2). \tag{2.34}$$

Note that the Frenet frame can be described as $\Phi_n = \mathrm{R}_{\psi_n}$. Then, by definition of K_n, we have the identity $\mathrm{R}_{\psi_n} = \mathrm{R}_{\psi_{n-1}} \mathrm{R}_{K_n}$, which is written as

$$\Phi_n = \Phi_{n-1} \begin{pmatrix} \cos K_n & -\sin K_n \\ \sin K_n & \cos K_n \end{pmatrix}, \qquad n = 1, \dots, N-1. \tag{2.35}$$

In the literature, (2.35) is usually presented as the definition of the discrete Frenet formula. However, in this thesis, we use an equivalent equation that is closely related to its continuous analogue. From (2.33) and (2.35), it can be seen that the Frenet frame satisfies that

$$\frac{\Phi_n - \Phi_{n-1}}{h} = \frac{\Phi_n + \Phi_{n-1}}{2} \begin{pmatrix} 0 & \kappa_n \\ \kappa_n & 0 \end{pmatrix}, \qquad n = 1, \dots, N-2. \tag{2.36}$$

which we defined as the **(discrete) Frenet formula**, by analogy with (2.11) in the smooth case.

Remark 2.10 — Let us see that (2.32) and (2.33) are well-defined. By definition of discrete regular curve, (2.24) in terms of the turning angle is written as

$$\det\left(\begin{pmatrix} \cos\psi_{n+1} \\ \sin\psi_{n+1} \end{pmatrix}, \begin{pmatrix} \cos\psi_n \\ \sin\psi_n \end{pmatrix} \right) \neq 0, \tag{2.37}$$

which is equivalent to $\sin K_n \neq 0$. Hence, $K_n \neq 0, \pm\pi, \dots$, and so on, implying that $\tan\left(\frac{K_n}{2}\right)$ is well-defined and non-zero.

Theorem 2.11 — *Given a map $\kappa_n \in \mathbb{R}$, $n = 1, \dots, N-2$, for every $h > 0$, there exists a discrete planar curve $\gamma_n \in \mathbb{R}^2$, $n = 0, \dots, N-1$, with step size h, such that κ_n is its discrete curvature. Furthermore, for each h, the curve is uniquely determined up to rigid transformations of the plane.*

Proof. We proceed by explicitly constructing the curve. Firstly, for each $h > 0$, we compute $K_n = 2\arctan(h\kappa_n/2)$, $n = 1, \dots, N-2$. Then, from (2.31), the turning angle is obtained recursively,

$$\begin{cases} \psi_n = \psi_{n-1} + K_n, & n = 1, \dots, N-2, \\ \psi_0 = \psi_{\text{init}}, \end{cases} \tag{2.38}$$

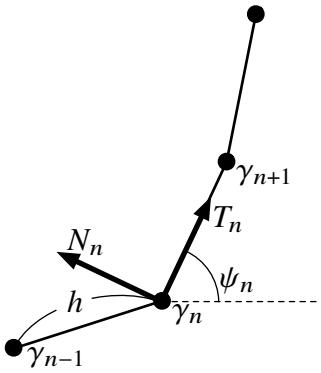

Figure 2.2: Representation of a discrete planar curve with step size h and its relation to the Frenet frame and the turning angle.

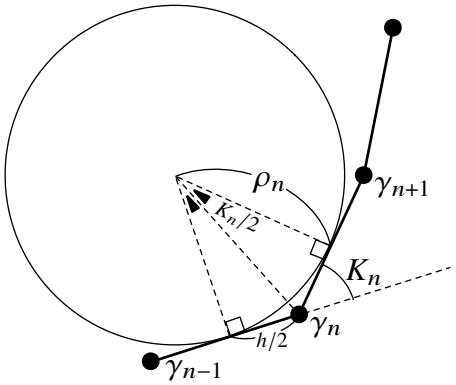

Figure 2.3: Representation of a discrete planar curve with step size h and its relation to the deflection angle and the radius of curvature.

for some $\psi_{\text{init}} \in \mathbb{R}$. Finally, from (2.28) and (2.30), we obtain the discrete curve,

$$\begin{cases} \gamma_n = \gamma_{n-1} + h\,{}^{\mathrm{t}}(\cos\psi_{n-1}, \sin\psi_{n-1}), & n = 1, \dots, N-1, \\ \gamma_0 = {}^{\mathrm{t}}(x_{\text{init}}, y_{\text{init}}), \end{cases} \tag{2.39}$$

for some constants x_{init}, $y_{\text{init}} \in \mathbb{R}$. For the second part, by the previous construction, it is clear that two given discrete curve, with step size h, must have the same deflection angle. Hence, they differ only in the choice of the constants $\{x_{\text{init}}, y_{\text{init}}, \psi_{\text{init}}\}$, which are associated to rigid transformations of the plane. □

Corollary 2.12 — *Consider a map $\psi_n \in \mathbb{R}$, $n = 0, \dots, N-2$, satisfying that*

$$\psi_n \neq \psi_{n-1}, \qquad n = 1, \dots, N-2. \tag{2.40}$$

Then, for every $h > 0$ there exists a discrete planar curve $\gamma_n \in \mathbb{R}^2$, $n = 0, \dots, N-1$, with step size h, such that ψ_n is its turning angle. Furthermore, for each h, the curve is uniquely determined up to translations of the plane.

Corollary 2.13 — *Given a map $K_n \in \mathbb{R}$, $n = 1, \dots, N-2$, there exists a discrete planar curve $\gamma_n \in \mathbb{R}^2$, $n = 0, \dots, N-1$ such that K_n is its deflection. Furthermore, the curve is uniquely determined up to rigid transformations of the plane and scale transformations.*

2.2.1 Continuum limit of discrete objects

The discrete objects defined in this thesis depend on the step size h, which is used to recover their respective continuous counterpart when the limit of h going to

zero is taken, denoted as $h \to 0$. In a general setting, we proceed as follows: For a given discrete object f_n, which depends on h, we assume that there exists a smooth function $\hat{f}$ that extends f_n, for every $h > 0$, such that

$$\hat{f}(nh) = f_n. \tag{2.41}$$

Then, we investigate different properties of f_n from $\hat{f}$ and its Taylor expansions at $h = 0$. We will frequently use the following expressions:

$$f_n = \hat{f}(s), \tag{2.42}$$

$$f_{n-1} = \hat{f}(s-h) = \hat{f}(s) - h\hat{f}'(s) + \frac{1}{2}h^2\hat{f}''(s) + O(h^3), \tag{2.43}$$

$$f_{n+1} = \hat{f}(s+h) = \hat{f}(s) + h\hat{f}'(s) + \frac{1}{2}h^2\hat{f}''(s) + O(h^3), \tag{2.44}$$

and so on, where $s := nh$. When it is clear by the context, we denote the smooth function simply as f, instead of $\hat{f}$. In some circumstances, special attention should be paid and we possibly need to scale appropriately the discrete object or its parameters in order to obtain a well-defined limit. For example, as $h \to 0$ we have that

$$\gamma_{n+1} - \gamma_n = h\gamma'(s) + O(h^2) \xrightarrow[h\to 0]{} 0, \tag{2.45}$$

however

$$\frac{1}{h}(\gamma_{n+1} - \gamma_n) \xrightarrow[h\to 0]{} \gamma'(s). \tag{2.46}$$

As the last part of this chapter, let us see some relations between the smooth and discrete objects defined in Section 2.1 and Section 2.2, respectively. We defined a discrete curve to satisfy that $\|\gamma_{n+1} - \gamma_n\| = h$, then its continuum limit gives an arc length parameterized curve,

$$\|\gamma_{n+1} - \gamma_n\| = h \xrightarrow[h\to 0]{} \|\gamma'(s)\| = 1. \tag{2.47}$$

Furthermore, for the tangent vector we have that

$$T_n = \frac{\gamma_{n+1} - \gamma_n}{\|\gamma_{n+1} - \gamma_n\|} \xrightarrow[h\to 0]{} \frac{\gamma'(s)}{\|\gamma'(s)\|} = \gamma'(s) = T(s). \tag{2.48}$$

Finally, for the discrete curvature we can see that

$$\kappa_n = \frac{2}{h}\tan\left(\frac{\psi_n - \psi_{n-1}}{2}\right) \xrightarrow[h\to 0]{} \psi'(s) = \kappa(s), \tag{2.49}$$

where we have used that the underlying smooth curve is parameterized by arc length. In conclusion, we note that Definition 2.8 provides a discrete curve that is in correspondence to an arc length parameterized curve in the limit $h \to 0$, and the quantities defined in the discrete framework correspond to the equivalent quantities in the continuous framework, for arc length parameterized curves.

Chapter 3

Fairing to Euler's elasticae

This chapter addresses solely the Euler's elastica. In Section 3.1 and Section 3.2 we review and present definitions of the smooth and discrete case, collecting the information on variational formulations, exact solutions, and continuum limits. In Section 3.3, we present a detailed account of the fairing method from a general discrete planar curve to the discrete Euler's elastica. Explicit expressions are given in terms of the Jacobi elliptic functions, and for various formulas the readers may refer to [27, 38], for example. Part of the content of this chapter is included in [13].

3.1 Euler's elastica

Historically, the term elastica comes from the shape that thin rods of a flexible material acquire when they are bent [28]. From a mathematical point of view, the **Euler's elastica** (or simply referred to as the elastica) is defined as a critical point of the *elastic energy* [26]

$$E[\gamma] = \int_0^L (\kappa(s))^2 \, \mathrm{d}s, \tag{3.1}$$

with respect to variations with fixed endpoints and fixed tangent vectors at the endpoints, under the condition of preserving the total length. The Euler-Lagrange equation yields the following differential equations for the curvature and the turning angle:

Proposition 3.1 — *The curvature κ of an Euler's elastica satisfies*

$$\kappa'' + \frac{1}{2}\kappa^3 - \lambda\kappa = 0, \tag{3.2}$$

for some constant $\lambda \in \mathbb{R}$. Moreover, up to a rigid rotation of the plane, the turning angle ψ satisfies

$$\psi'' + \mu \sin \psi = 0, \tag{3.3}$$

for some constant $\mu > 0$.

Proof. Derivation of (3.2) is given in various literature, such as [3, 5, 43]. We show a concise derivation using the variation of the tangent vector. Consider the functional

$$S[T] = \int_0^L (\langle T', T' \rangle + c\langle T, T \rangle + \langle a, T \rangle)\, \mathrm{d}s, \tag{3.4}$$

which is obtained from (3.1) after incorporating the constraints

$$\begin{cases} \|T'\| = \text{const.}, \\ \gamma(L) - \gamma(0) = \text{const.}, \end{cases} \tag{3.5}$$

with $c = c(s) \in \mathbb{R}$ and $a \in \mathbb{R}^2$ being the corresponding Lagrange multipliers. The variation of S is calculated by using the Frenet formula (2.11) as

$$\begin{aligned} \delta S &= \int_0^L (2\langle T', \delta T' \rangle + 2c(s)\langle T, \delta T \rangle + \langle a, \delta T \rangle)\, \mathrm{d}s \\ &= 2\langle T', \delta T \rangle \Big|_0^L + 2 \int_0^L \left\langle (\kappa^2 + c(s))T - \kappa' N + \frac{a}{2}, \delta T \right\rangle \mathrm{d}s. \end{aligned} \tag{3.6}$$

The first term is the boundary term, which vanishes due to the boundary condition, and the second term gives the Euler-Lagrange equation

$$(\kappa^2 + c)\, T - \kappa' N + \frac{a}{2} = 0. \tag{3.7}$$

Then, the scalar product of (3.7) with N gives

$$-\kappa' + \frac{1}{2}\langle a, N \rangle = 0. \tag{3.8}$$

On the one hand, the result of multiplying (3.8) by κ' is integrated to obtain

$$\frac{\kappa^2}{2} - \lambda = \frac{1}{2}\langle a, T \rangle, \tag{3.9}$$

where $\lambda \in \mathbb{R}$ is a constant of integration. On the other hand, differentiating (3.8) and using that $N' = -\kappa T$ gives

$$\kappa'' = -\frac{\kappa}{2}\langle a, T \rangle. \tag{3.10}$$

Hence, eliminating $\langle a, T\rangle$ from equations (3.9) and (3.10) yields

$$\kappa'' + \kappa\left(\frac{\kappa^2}{2} - \lambda\right) = 0, \tag{3.11}$$

which is nothing but (3.2). For the second part, we consider the functional

$$\tilde{S}[\psi] = \int_0^L \left((\psi')^2 + \left\langle a, \begin{pmatrix}\cos\psi \\ \sin\psi\end{pmatrix}\right\rangle\right) \mathrm{d}s, \tag{3.12}$$

which is obtained from (3.1) after incorporating the constraint $\gamma(L)-\gamma(0) = \text{const.}$, written in terms of the turning angle, with $a \in \mathbb{R}^2$ being the corresponding Lagrange multiplier. Note that

$$\left\langle a, \begin{pmatrix}\cos\psi \\ \sin\psi\end{pmatrix}\right\rangle = 2\mu\cos(\psi - \phi), \tag{3.13}$$

for some constants $\mu > 0$ and $\phi \in \mathbb{R}$, thus

$$\tilde{S}[\psi] = \int_0^L \Big((\psi')^2 + 2\mu\cos(\psi - \phi)\Big)\,\mathrm{d}s. \tag{3.14}$$

The Euler-Lagrange equation is readily obtained as

$$\psi'' + \mu\sin(\psi - \phi) = 0, \tag{3.15}$$

which is nothing but (3.3) after applying a rigid rotation of the plane that shifts ψ to $\psi + \phi$. □

Remark 3.2 — Both defining equations for the Euler's elastica are equivalent, in the sense that (3.2) is derived from (3.3) as follows: The result of multiplying (3.3) by ψ' is integrated to obtain

$$\frac{1}{2}(\psi')^2 = \mu\cos\psi + \lambda, \tag{3.16}$$

where $\lambda \in \mathbb{R}$ is a constant of integration. Then, differentiating (3.3) and using (3.16), to eliminate the term with $\cos\psi$, yields

$$\psi''' = \left(-\frac{1}{2}(\psi')^2 + \lambda\right)\psi', \tag{3.17}$$

which is (3.2) written in terms of $\psi' = \kappa$.

Remark 3.3 — Equations (3.2) and (3.3) can be seen as travelling-wave reductions of the (focusing) modified KdV equation,

$$\frac{\partial \kappa}{\partial t} + \frac{3}{2}\kappa^2 \frac{\partial \kappa}{\partial s} + \frac{\partial^3 \kappa}{\partial s^3} = 0, \tag{3.18}$$

and the sine-Gordon equation,

$$\frac{\partial^2 \psi}{\partial s \partial y} = \sin \psi, \tag{3.19}$$

respectively, where the former describes the integrable deformation of planar curves [12, 21].

It is known that the differential equations (3.2) and (3.3) can be solved in terms of the Jacobi elliptic functions. In the literature, the solutions are often constructed from their first integral,

$$(\kappa')^2 + \frac{\kappa^4}{2} - \lambda \kappa^2 = c, \tag{3.20}$$

$$\frac{1}{2}(\psi')^2 - \mu \cos \psi = \lambda, \tag{3.21}$$

respectively, where $c \in \mathbb{R}$ is a constant. We present the solutions and verify them by using formulas for the differential equations of the Jacobi elliptic functions. We note that, depending on the boundary or initial conditions, there are two families of solutions: Euler's elasticae with inflection points and Euler's elasticae without inflection points. When consider necessary, we refer to them as **WI** (with inflection) and **NI** (no inflection), respectively. Some examples of different Euler's elasticae are shown in Figure 3.1.

Proposition 3.4 — *The curvature and the turning angle of an Euler's elastica can be expressed in terms of the Jacobi elliptic functions as follows:*

[WI]

$$\kappa(s) = 2k\sqrt{\mu}\, \mathrm{cn}\big(\sqrt{\mu}(s + s_0); k\big), \tag{3.22}$$

$$\sin \frac{\psi(s)}{2} = k\, \mathrm{sn}\big(\sqrt{\mu}(s + s_0); k\big), \qquad \mu = \frac{\lambda}{2k^2 - 1}, \tag{3.23}$$

[NI]

$$\kappa(s) = 2k^{-1}\sqrt{\mu}\, \mathrm{dn}\Big(k^{-1}\sqrt{\mu}(s + s_0); k\Big), \tag{3.24}$$

$$\sin \frac{\psi(s)}{2} = \mathrm{sn}\Big(k^{-1}\sqrt{\mu}(s + s_0); k\Big), \qquad \mu = \frac{\lambda}{2k^{-2} - 1}, \tag{3.25}$$

for the elastica with or without inflection points, respectively, where $\mu > 0$, $s_0 \in \mathbb{R}$, *and* $k \in (0, 1)$ *are constants.*

Remark 3.5 — The Jacobi elliptic functions admit an analytic continuation to modules $k \geq 1$, see, for example, [27, 38]. In particular, the following formulas hold:

$$\mathrm{sn}(u;k) = k^{-1}\,\mathrm{sn}(ku;k^{-1}), \tag{3.26}$$

$$\mathrm{cn}(u;k) = \mathrm{dn}(ku;k^{-1}), \tag{3.27}$$

$$\mathrm{dn}(u;k) = \mathrm{cn}(ku;k^{-1}). \tag{3.28}$$

Taking this into account, the cases [WI] and [NI] are regarded as one, and the range of k is extended to $[0,\infty]$.

proof of Proposition 3.4. To verify that (3.22) and (3.24) are solutions of (3.2), for [WI] and [NI], we simply use the formula for the second derivative of the cn and dn functions [38],

$$\frac{\mathrm{d}^2}{\mathrm{d}u^2}\,\mathrm{cn}(u;k) = (2k^2-1)\,\mathrm{cn}(u;k) - 2k^2(\mathrm{cn}(u;k))^3, \tag{3.29}$$

$$\frac{\mathrm{d}^2}{\mathrm{d}u^2}\,\mathrm{dn}(u;k) = (2-k^2)\,\mathrm{dn}(u;k) - 2(\mathrm{dn}(u;k))^3, \tag{3.30}$$

respectively. To verify that (3.23) and (3.23) are solutions of (3.3), we proceed as shown in Example 2.7, where case [NI] was depicted. Case [WI] is verified in a similar manner, using the identities

$$(\mathrm{dn}(u;k))^2 + k^2(\mathrm{sn}(u;k))^2 = 1, \tag{3.31}$$

$$\frac{\mathrm{d}}{\mathrm{d}u}\,\mathrm{sn}(u;k) = \mathrm{cn}(u;k)\,\mathrm{dn}(u;k), \tag{3.32}$$

$$\frac{\mathrm{d}}{\mathrm{d}u}\,\mathrm{cn}(u;k) = -\,\mathrm{sn}(u;k)\,\mathrm{dn}(u;k). \tag{3.33}$$

□

3.2 Integrable discrete Euler's elastica

The **discrete Euler's elastica** [3, 5, 19, 44] is defined as a discrete planar curve with step size h that is a critical point of the functional

$$\begin{aligned} E_d &= \sum_{n=1}^{N-2} \frac{2}{h} \log\left(1 + \frac{h^2}{4}\kappa_n^2\right) \\ &= -\sum_{n=1}^{N-2} \frac{2}{h} \log\left(1 + \langle T_{n-1}, T_n\rangle\right) + \text{const.}, \end{aligned} \tag{3.34}$$

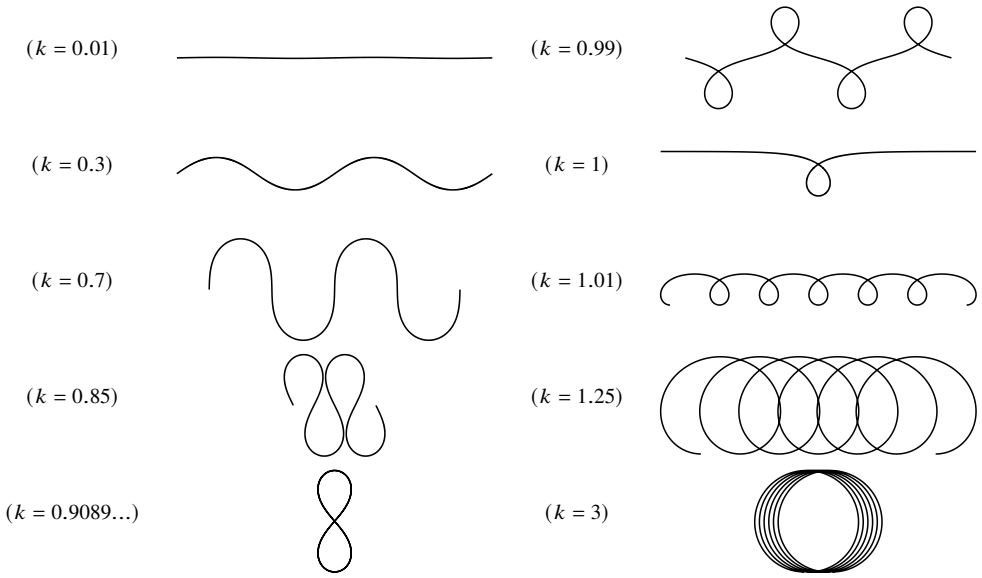

Figure 3.1: Typical examples of Euler's elasticae. The case $k = 0.9089...$ is the solution of $2E(k) = K(k)$, where $K(k)$ and $E(k)$ are the complete elliptical integrals of first and second kind, respectively. The equation $2E(k) = K(k)$ is related with the periodicity of the Euler's elastica curve.

with respect to variations with fixed endpoints and end edges. The equivalence between both expressions come from the relation

$$1 + \frac{h^2}{4}\kappa_n^2 = \frac{2}{1 + \langle T_n, T_{n-1}\rangle}, \tag{3.35}$$

which can be seen as a trigonometric identity after replacing all the quantities in terms of the turning angle ψ_n. As mentioned in [3], the functional E_d can be regarded as a discrete analogue of the elastic energy (3.1). This can be seen as follows: On the one hand, it is known that the *bending moment* M of a thin rod is proportional to the curvature [26], $M \propto \kappa$. On the other hand, assume that the curvature of two consecutive segments of length h is given by $\kappa(\varepsilon) = 2\tan(\varepsilon/2)/h$, where ε is the deflection between both segments. Then, we find that the total work exerted at each inner vertex is

$$\int_0^{K_n} M(\varepsilon)\,\mathrm{d}\varepsilon \propto \frac{2}{h}\log\left(1 + \frac{h^2}{4}(\kappa(K_n))^2\right). \tag{3.36}$$

Proposition 3.6 — *The curvature of a discrete Euler's elastica satisfies*

$$\kappa_{n+1} + \kappa_{n-1} = \frac{\alpha\kappa_n}{1 + \frac{h^2}{4}\kappa_n^2}, \tag{3.37}$$

for some constant $\alpha \in \mathbb{R}$.

Proof. Following [3, 5], consider the functional

$$S_d = \sum_{n=1}^{N-2} \left(\frac{2}{h} \log(1 + \langle T_{n-1}, T_n \rangle) + c_{n-1} \langle T_{n-1}, T_{n-1} \rangle + h \langle a, T_{n-1} \rangle \right) \tag{3.38}$$

which is obtained from (3.34) after incorporating the constraints

$$\begin{cases} \|\gamma_n - \gamma_{n-1}\| = \text{const.}, \\ \gamma_N - \gamma_0 = \text{const.}, \end{cases} \tag{3.39}$$

with $c_n \in \mathbb{R}$ and $a \in \mathbb{R}^2$ being the corresponding Lagrange multipliers. Define $L(T_{n-1}, T_n)$ such that $S_d = \sum_{n=1}^{N-2} L(T_{n-1}, T_n)$. Then, it is easy to see that the discrete Euler-Lagrange equation,

$$\frac{\partial}{\partial T_n} L(T_{n-1}, T_n) + \frac{\partial}{\partial T_n} L(T_n, T_{n+1}) = 0, \tag{3.40}$$

obtained from variations with fixed endpoints ($\delta T_0 = 0$ and $\delta T_{N-2} = 0$), gives

$$\frac{2}{h} \frac{T_{n-1}}{1 + \langle T_{n-1}, T_n \rangle} + \frac{2}{h} \frac{T_{n+1}}{1 + \langle T_n, T_{n+1} \rangle} + 2c_n T_n + ha = 0. \tag{3.41}$$

From the discrete Frenet formula (2.36) written in terms of T_n and N_n,

$$\frac{T_n - T_{n-1}}{h} = \kappa_n \frac{N_n + N_{n-1}}{2}, \tag{3.42}$$

$$\frac{N_n - N_{n-1}}{h} = -\kappa_n \frac{T_n + T_{n-1}}{2}, \tag{3.43}$$

we obtain

$$\frac{2}{h} \frac{\langle T_n, N_n \rangle}{1 + \langle T_n, T_{n+1} \rangle} = \kappa_{n+1}, \tag{3.44}$$

$$\frac{2}{h} \frac{\langle T_{n-1}, N_n \rangle}{1 + \langle T_{n-1}, T_n \rangle} = -\kappa_n. \tag{3.45}$$

Then, using (3.44) and (3.45) in (3.41) gives

$$\kappa_n - \kappa_{n+1} = h \langle a, N_n \rangle. \tag{3.46}$$

On the other hand, from (3.42) and (3.46) we have

$$\langle a, T_n \rangle - \langle a, T_{n-1} \rangle = -\frac{1}{2} \kappa_n \kappa_{n+1} + \frac{1}{2} \kappa_{n-1} \kappa_n, \tag{3.47}$$

which implies that there exists a constant $\lambda \in \mathbb{R}$ such that

$$\langle a, T_n \rangle = -\frac{1}{2}\kappa_n \kappa_{n+1} + \lambda. \tag{3.48}$$

Finally, from (3.42), (3.46) and (3.48), we obtain

$$(\kappa_{n+1} + \kappa_{n-1})\left(1 + \frac{h^2}{4}\kappa_n^2\right) = (2 + h^2\lambda)\kappa_n, \tag{3.49}$$

that is exactly (3.37) with $\alpha = 2 + h^2\lambda$. □

By using techniques similar to the ones shown in [45], we obtained explicit solutions to (3.37) from its discrete first integral,

$$\kappa_{n+1}^2 + \kappa_n^2 - \alpha\kappa_{n+1}\kappa_n + \frac{h^2}{4}\kappa_{n+1}^2\kappa_n^2 = C, \tag{3.50}$$

where $C \in \mathbb{R}$ is a constant. Here, we avoid the very long computation required to obtain the explicit solutions. We simply present and verify them by using the addition formulas for the Jacobi elliptic functions. Note that the following solutions are in correspondence to (3.22) and (3.24) in the continuum limit. Figure 3.2 illustrates some typical examples of both smooth and discrete elasticae.

Proposition 3.7 — *The curvature of a discrete Euler's elastica can be expressed in terms of the Jacobi elliptic functions as follows:*

[WI]

$$\kappa_n = \frac{2k\,\mathrm{sn}(z;k)}{h\,\mathrm{dn}(z;k)}\,\mathrm{cn}(zn+q;k), \qquad \alpha = \frac{2\,\mathrm{cn}(z;k)}{(\mathrm{dn}(z;k))^2}, \tag{3.51}$$

[NI]

$$\kappa_n = \frac{2\,\mathrm{sn}(k^{-1}z;k)}{h\,\mathrm{cn}(k^{-1}z;k)}\,\mathrm{dn}(k^{-1}(zn+q);k), \qquad \alpha = \frac{2\,\mathrm{dn}(k^{-1}z;k)}{(\mathrm{cn}(k^{-1}z;k))^2}. \tag{3.52}$$

where $z, q \in \mathbb{R}$ and $k > 0$ are constants.

Proof. By direct computation, using the addition formulas for the dn and cn functions [38], we verify that (3.51) and (3.52) are solutions of (3.37). For [WI], we use the formula

$$\mathrm{cn}(u+v) + \mathrm{cn}(u-v) = \frac{\frac{2\,\mathrm{cn}\,v}{\mathrm{dn}^2\,v}\,\mathrm{cn}\,u}{1 + \frac{k^2\,\mathrm{sn}^2\,v}{\mathrm{dn}^2\,v}\,\mathrm{cn}^2\,u}, \tag{3.53}$$

where for simplicity in the notation we omitted the module k, as in $\operatorname{cn} u \equiv \operatorname{cn}(u;k)$ and similarly for the other quantities. Then, by choosing

$$\begin{cases} u = zn + q, \\ v = z, \end{cases} \tag{3.54}$$

we satisfy (3.37), with

$$\kappa_n = A \operatorname{cn}(u;k), \quad A = \frac{2k \operatorname{sn} v}{h \operatorname{dn} v}, \quad \alpha = \frac{2 \operatorname{cn} v}{\operatorname{dn}^2 v}, \tag{3.55}$$

which proves (3.51). For [NI] we proceed analogously, from the formula

$$\operatorname{dn}(u+v) + \operatorname{dn}(u-v) = \frac{\frac{2 \operatorname{dn} v}{\operatorname{cn}^2 v} \operatorname{dn} u}{1 + \frac{\operatorname{sn}^2 v}{\operatorname{cn}^2 v} \operatorname{dn}^2 u}, \tag{3.56}$$

and by choosing

$$\begin{cases} u = k^{-1}(zn + q), \\ v = k^{-1} z. \end{cases} \tag{3.57}$$

This yields (3.37), with

$$\kappa_n = A \operatorname{dn}(u;k), \quad A = \frac{2 \operatorname{sn} v}{h \operatorname{cn} v}, \quad \alpha = \frac{2 \operatorname{dn} v}{\operatorname{cn}^2 v}, \tag{3.58}$$

which proves (3.52). □

Remark 3.8 — By comparing (3.22) and (3.51), we can fix the values of z and q such that there exists a constant Ω satisfying that $\kappa_n = \kappa(\Omega n)$. Indeed, the following constraints must be satisfied:

$$z = \operatorname{sn}^{-1}\left(\sqrt{\frac{\mu h^2}{\mu h^2 k^2 + 1}}; k\right), \quad q = \sqrt{\mu} s_0, \quad \Omega = \frac{z}{\sqrt{\mu}}. \tag{3.59}$$

There is also a similar relationship between equations (3.24) and (3.52). The relation $\kappa_n = \kappa(\Omega n)$ implies that the discrete curvature κ_n is an *exact discretization* [30] of the smooth curvature $\kappa(s)$.

Remark 3.9 (Continuum limit) — By putting $\alpha = 2 + h^2\lambda$ and $nh = s$, the difference equation (3.37) yields the differential equation (3.2) in the continuum limit $h \to 0$. On the level of solutions, (3.51) and (3.52), with the parameterization of z and q given by

$$\begin{cases} z = h\sqrt{\mu}, \\ q = s_0\sqrt{\mu}, \end{cases} \tag{3.60}$$

are consistent in the continuum limit with (3.22) and (3.24), respectively.

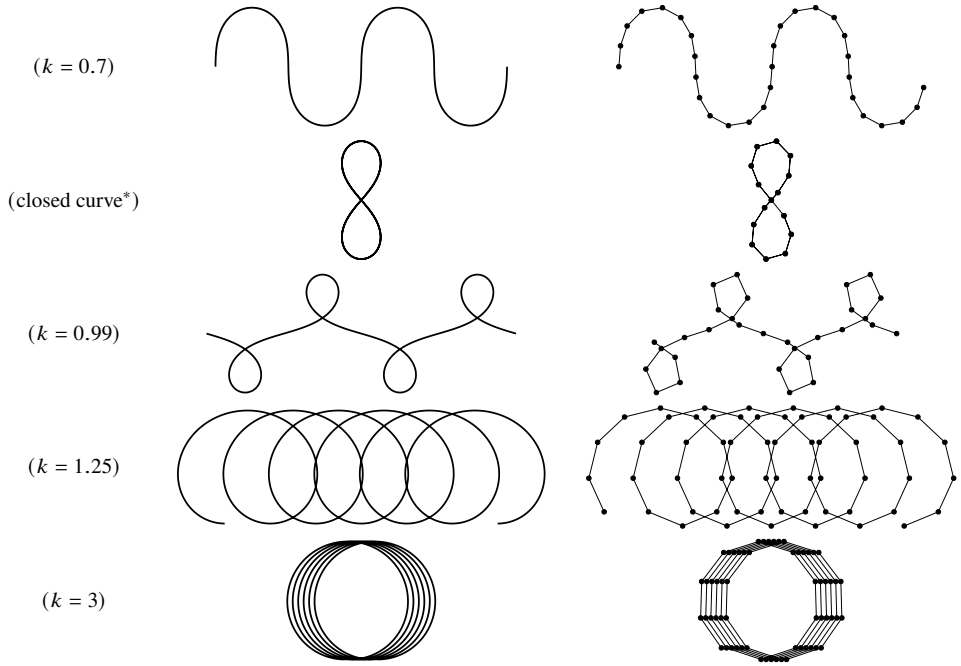

Figure 3.2: Typical examples of smooth and discrete elasticae. The closed curve case has different values of k for each value of z, reaching $k = 0.9089...$ in the continuum limit.

Remark 3.10 — Equation (3.37) is also known as the McMillan map, which is a special case of the Quispel-Roberts-Thompson (QRT) map solved by elliptic functions [40]. It can also be regarded as an autonomous version of a discrete Painlevé II equation [24, 25, 41]

Remark 3.11 — It is known that position vectors of both smooth and discrete elasticae admit explicit formulas in terms of the elliptic theta functions [33, 37]. However, those results are not used in this thesis.

3.2.1 Discrete Euler's elastica in terms of a potential function

In this section, we present a different approach to the discrete Euler's elastica [44], and we show that is, indeed, compatible with the previous definition. Firstly, following [21], we define the **potential angle** θ_n such that

$$\psi_n = \frac{\theta_{n+1} + \theta_n}{2}. \tag{3.61}$$

Note that the potential angle has one degree of freedom for a given discrete curve. In this context, the discrete curvature is written as

$$\kappa_n = \frac{2}{h}\tan\left(\frac{\theta_{n+1}-\theta_{n-1}}{4}\right). \tag{3.62}$$

Following [44], we present the variational formulation for the discrete Euler's elastica, but we use the potential angle instead of the turning angle as it was originally written. This change makes this theory compatible with the discrete isoperimetric and equidistant deformation of discrete planar curves, and is crucial to prove the equivalence with the previous construction.

Proposition 3.12 — *Suppose that $\theta_n \in \mathbb{R}$, $n = 0, \dots, N-1$, is a critical point of the functional*

$$\tilde{S}_d = \sum_{n=0}^{N-2} \cos\left(\frac{\theta_{n+1}-\theta_n}{2}\right) - \epsilon\cos\left(\frac{\theta_{n+1}+\theta_n}{2}\right), \tag{3.63}$$

for some constant $\epsilon > 0$, with respect to variations of θ_n with fixed endpoints. Then, the following holds:

(1) The Euler-Lagrange equation is

$$\sin\left(\frac{\theta_{n+1}-2\theta_n+\theta_{n-1}}{4}\right) + \epsilon\sin\left(\frac{\theta_{n+1}+2\theta_n+\theta_{n-1}}{4}\right) = 0. \tag{3.64}$$

(2) There exists a conserved quantity

$$\cos\left(\frac{\theta_{n+1}-\theta_n}{2}\right) + \epsilon\cos\left(\frac{\theta_{n+1}+\theta_n}{2}\right) = \Lambda, \tag{3.65}$$

where $\Lambda \in \mathbb{R}$ is a constant.

(3) For $h > 0$, the discrete curvature κ_n obtained from (3.62) satisfies (3.37) with $\alpha = 2(1-\epsilon^2)/\Lambda^2$. Therefore, the discrete curve obtained from this construction is a discrete Euler's elastica.

Proof. For (1), let $L(\theta_n, \theta_{n+1})$ be such that $\tilde{S}_d = \sum_{n=1}^{N-2} L(\theta_n, \theta_{n+1})$. Then, the Euler-Lagrange equation,

$$\frac{\partial}{\partial\theta_n}L(\theta_{n-1},\theta_n) + \frac{\partial}{\partial\theta_n}L(\theta_n,\theta_{n+1}) = 0, \tag{3.66}$$

is expressed as

$$0 = \cos\left(\frac{\theta_{n+1} - \theta_{n-1}}{4}\right)\left[\sin\left(\frac{\theta_{n+1} - 2\theta_n + \theta_{n-1}}{4}\right) + \epsilon \sin\left(\frac{\theta_{n+1} + 2\theta_n + \theta_{n-1}}{4}\right)\right], \tag{3.67}$$

which gives (3.64). For (2), we multiply (3.64) by $\sin(\frac{\theta_{n+1}-\theta_{n-1}}{4})$, use the product-to-sum formula, and rearrange the terms to obtain

$$\cos\left(\frac{\theta_{n+1} - \theta_n}{2}\right) + \epsilon \cos\left(\frac{\theta_{n+1} + \theta_n}{2}\right) = \cos\left(\frac{\theta_n - \theta_{n-1}}{2}\right) + \epsilon \cos\left(\frac{\theta_n + \theta_{n-1}}{2}\right), \tag{3.68}$$

which implies (3.65). For (3), we introduce the quantity

$$\varphi_n = \frac{\theta_{n+1} - \theta_n}{2}, \tag{3.69}$$

for simplicity in the notation. In this case, note that $K_n = \psi_n - \psi_{n-1} = \varphi_n + \varphi_{n-1}$, thus (3.64) and (3.65) are rewritten as

$$\sin\left(\frac{\varphi_n - \varphi_{n-1}}{2}\right) = -\epsilon \sin\left(\frac{\psi_n + \psi_{n-1}}{2}\right), \tag{3.70}$$

$$\cos\varphi_n + \epsilon \cos\psi_n = \Lambda, \tag{3.71}$$

respectively. From (3.70) and (3.71), we obtain

$$\tan\frac{K_{n-1}}{2} = \frac{\sin\varphi_{n-1} + \epsilon \sin\psi_{n-1}}{\Lambda}, \tag{3.72}$$

$$\tan\frac{K_{n+1}}{2} = \frac{\sin\varphi_n - \epsilon \sin\psi_n}{\Lambda}. \tag{3.73}$$

Then, we combine (3.72) and (3.73), and use the sum-to-product formula to obtain

$$\Lambda\left(\tan\frac{K_{n+1}}{2} + \tan\frac{K_{n-1}}{2}\right) = 2\sin\frac{K_n}{2}\left[\cos\left(\frac{\varphi_n - \varphi_{n-1}}{2}\right) - \epsilon \cos\left(\frac{\psi_n + \psi_{n-1}}{2}\right)\right]. \tag{3.74}$$

On a separate note, consider

$$\cos\left(\frac{\varphi_n - \varphi_{n-1}}{2}\right) + \epsilon \cos\left(\frac{\psi_n + \psi_{n-1}}{2}\right) = \cos\frac{K_n}{2}(\cos\varphi_n + \epsilon\cos\psi_n) + \sin\frac{K_n}{2}(\sin\varphi_n + \epsilon\sin\psi_n), \tag{3.75}$$

which is a trigonometric identity, that is expressed as

$$\cos\left(\frac{\varphi_n-\varphi_{n-1}}{2}\right)+\epsilon\cos\left(\frac{\psi_n+\psi_{n-1}}{2}\right)=\frac{\Lambda}{\cos\frac{K_n}{2}}, \tag{3.76}$$

by means of (3.71) and (3.72). From the square of (3.70), we have

$$\cos^2\left(\frac{\varphi_n-\varphi_{n-1}}{2}\right)-\epsilon^2\cos^2\left(\frac{\psi_n+\psi_{n-1}}{2}\right)=1-\epsilon^2, \tag{3.77}$$

which is rewritten as

$$\cos\left(\frac{\varphi_n-\varphi_{n-1}}{2}\right)-\epsilon\cos\left(\frac{\psi_n+\psi_{n-1}}{2}\right)=\frac{1-\epsilon^2}{\Lambda}\cos\frac{K_n}{2} \tag{3.78}$$

by means of (3.76). Finally, from (3.74) and (3.78) we obtain

$$\tan\frac{K_{n+1}}{2}+\tan\frac{K_{n-1}}{2}=\frac{1-\epsilon^2}{\Lambda^2}\frac{2\tan\frac{K_n}{2}}{1+\tan^2\frac{K_n}{2}}. \tag{3.79}$$

Hence, from the definition of discrete curvature, (3.79) is equivalent to equation (3.37) with $\alpha=2(1-\epsilon^2)/\Lambda^2$. □

Remark 3.13 (Continuum limit) — Proposition 3.12 provides discrete analogues for equations (3.3) and (3.16). In fact, by putting

$$\Lambda=1-\frac{h^2}{4}\lambda,\quad \epsilon=\frac{h^2}{4}\mu,\quad s=nh, \tag{3.80}$$

equations (3.64) and (3.65) yield equations (3.3) and (3.16) in the continuum limit $h\to 0$.

In [44], an explicit solution of (3.64) in terms of the Jacobi elliptic functions is derived by using the Hirota's bilinear form [16]. We present that solution and a verification by means of the addition formulas for the Jacobi elliptic functions.

Proposition 3.14 — *The following functions satisfy* (3.64)*:*

[WI]

$$\sin\frac{\theta_n}{2}=k\,\mathrm{sn}(zn+q;k),\qquad \mathrm{cn}(z;k)=\frac{1-\epsilon}{1+\epsilon}, \tag{3.81}$$

[NI]

$$\sin\frac{\theta_n}{2}=\mathrm{sn}(k^{-1}(zn+q);k),\qquad \mathrm{dn}(k^{-1}z;k)=\frac{1-\epsilon}{1+\epsilon}, \tag{3.82}$$

where $z,q\in\mathbb{R}$*, and* $k>0$ *are constants.*

Proof. Let us see that these explicit equations satisfy (3.65), which can be expanded as

$$(1+\epsilon)\cos\frac{\theta_{n+1}}{2}\cos\frac{\theta_n}{2}+(1-\epsilon)\sin\frac{\theta_{n+1}}{2}\sin\frac{\theta_n}{2}=\Lambda. \tag{3.83}$$

For [WI], consider

$$\begin{cases} u = zn+q, \\ v = z, \end{cases} \tag{3.84}$$

so that (3.83) is rewritten as

$$(1+\epsilon)\,\mathrm{dn}(u+v;k)\,\mathrm{dn}(u;k)+(1-\epsilon)k^2\,\mathrm{sn}(u+v;k)\,\mathrm{sn}(u;k)=\Lambda. \tag{3.85}$$

Then, by means of the addition formulas for the sn and dn functions, the later expression becomes an identity if $\mathrm{cn}(z;k)=(1-\epsilon)/(1+\epsilon)$, and Λ is consistently reduced to $\Lambda=(1+\epsilon)\,\mathrm{dn}(z;k)$. Analogously, for [NI] we consider

$$\begin{cases} u = k^{-1}(zn+q), \\ v = k^{-1}z, \end{cases} \tag{3.86}$$

so that (3.83) is rewritten as

$$(1+\epsilon)\,\mathrm{cn}(u+v;k)\,\mathrm{cn}(u;k)+(1-\epsilon)\,\mathrm{sn}(u+v;k)\,\mathrm{sn}(u;k)=\Lambda, \tag{3.87}$$

which becomes an identity if $\mathrm{dn}(k^{-1}z;k)=(1-\epsilon)/(1+\epsilon)$, and Λ is consistently reduced to $\Lambda=(1+\epsilon)\,\mathrm{cn}(k^{-1}z;k)$. □

Remark 3.15 — Proposition 3.14, for the potential angle, and Proposition 3.7, for the discrete curvature, are in correspondence one with the other in the following sense.

[WI] — If the parameter α in (3.37) is given by

$$\alpha=2\frac{(1-\epsilon^2)}{\Lambda^2}=2\frac{\mathrm{cn}(z;k)}{\mathrm{dn}^2(z;k)}, \tag{3.88}$$

then (3.81) is in correspondence to (3.51).

[NI] — If the parameter α in (3.37) is given by

$$\alpha=2\frac{(1-\epsilon^2)}{\Lambda^2}=2\frac{\mathrm{dn}(k^{-1}z;k)}{\mathrm{cn}^2(k^{-1}z;k)}, \tag{3.89}$$

then (3.82) is in correspondence to (3.52). Furthermore, these relationships are verified by direct computation of the discrete curvature in terms of the potential angle, given by (3.62), using the explicit expressions (3.81) and (3.82), respectively.

Remark 3.16 (Continuum limit) — Continuum limits of equations (3.81) and (3.82) to equations (3.23) and (3.25), respectively, are obtained by putting $\epsilon = \frac{\mu}{4}h^2$ and taking the limit of $h \to 0$. This is consistent with Remark 3.9.

Remark 3.17 — Equation (3.64) can be seen as a reduction of two well-known equations:

(1) The discrete sine-Gordon equation [4, 16, 22],

$$\sin\left(\frac{\theta_{l+1}^{m+1} - \theta_l^{m+1} - \theta_{l+1}^m + \theta_l^m}{4}\right) = \frac{a}{b}\sin\left(\frac{\theta_{l+1}^{m+1} + \theta_l^{m+1} + \theta_{l+1}^m + \theta_l^m}{4}\right), \quad (3.90)$$

where a, b are lattice intervals. In fact, assuming that θ depends only on $n = l + m$, (3.90) is reduced to (3.64) with $\epsilon = -\frac{b}{a}$.

(2) The discrete potential modified KdV equation [17],

$$\tan\frac{\theta_{l+1}^{m+1} - \theta_l^m}{4} = \frac{b+a}{b-a}\tan\frac{\theta_l^{m+1} - \theta_{l+1}^m}{4}, \quad (3.91)$$

or equivalently

$$\sin\left(\frac{\theta_{l+1}^{m+1} - \theta_l^{m+1} + \theta_{l+1}^m - \theta_l^m}{4}\right) = \frac{a}{b}\sin\left(\frac{\theta_{l+1}^{m+1} + \theta_l^{m+1} - \theta_{l+1}^m - \theta_l^m}{4}\right), \quad (3.92)$$

which describes the isoperimetric and equidistant deformation of discrete planar curves [21, 32]. Equation (3.92) is transformed into (3.90) by the substitution $\theta_l^m \mapsto (-1)^m\theta_l^m$. In this sense, (3.64) can also be regarded as a reduction of the discrete potential modified KdV equation.

3.3 Fairing of discrete planar curves

In this section, we provide an algorithmic way to approximate a given discrete planar curve to a discrete elastica. Among the many possible discretizations for the elastica, the advantages of using the one shown in this thesis can be described as follows: The discrete objects are endowed with the same integrable structure as in their smooth counterpart, i.e., they possess several conserved quantities, can be obtained via a variational principle, and their explicit solutions are expressed in terms of the Jacobi elliptic functions. Moreover, it is known that variational integrators have controlled error in their solutions [9, 30, 39]. In particular, the explicit expression for the discrete curvature κ_n is an *exact discretization* of the

smooth curvature $\kappa(s)$ as discussed in Remark 3.9, and the potential function θ_n has the same functional shape as the smooth turning angle $\psi(s)$. From these observations, we expect this discretization to have good numerical properties.

Before describing the approximation method, we need the following expressions and results. Firstly, we incorporate the freedom of rotation. We do this by shifting the turning angle by a constant $\phi \in \mathbb{R}$, in all the expressions. In particular, the difference equation for the potential angle (3.64) goes to

$$\sin\left(\frac{\theta_{n+1} - 2\theta_n + \theta_{n-1}}{4}\right) + \frac{\mu h^2}{4} \sin\left(\frac{\theta_{n+1} + 2\theta_n + \theta_{n-1}}{4} - \phi\right) = 0, \tag{3.93}$$

where we put $\epsilon = \mu h^2/4$, with $\mu > 0$ a constant. Moreover, from Proposition 3.14, the explicit solutions of (3.93) become

[WI]

$$\sin\frac{\theta_n - \phi}{2} = k\,\mathrm{sn}(zn + q; k), \qquad \cos\frac{\theta_n - \phi}{2} = \mathrm{dn}(zn + q; k), \tag{3.94}$$

[NI]

$$\sin\frac{\theta_n - \phi}{2} = \mathrm{sn}(k^{-1}(zn + q); k), \quad \cos\frac{\theta_n - \phi}{2} = \mathrm{cn}(k^{-1}(zn + q); k), \tag{3.95}$$

where $k > 0$, $q, z \in \mathbb{R}$ are constants.

General discrete Euler's elastica segment

Given a potential function, a discrete Euler's elastica is computed recursively by

$$\begin{cases} \zeta_n^\Theta = \zeta_{n-1}^\Theta + h\begin{pmatrix} \cos\left(\frac{\theta_{n+1}-\phi}{2} + \frac{\theta_n-\phi}{2} - \phi\right) \\ \sin\left(\frac{\theta_{n+1}-\phi}{2} + \frac{\theta_n-\phi}{2} - \phi\right) \end{pmatrix}, & n = 1, \ldots, N-1, \\ \zeta_0^\Theta = \begin{pmatrix} x_0 \\ y_0 \end{pmatrix}, \end{cases} \tag{3.96}$$

where we use introduce the notation ζ^Θ for the Euler's elastica obtained from the parameters

$$\Theta := (x_0, y_0, h, \phi, z, q, k), \tag{3.97}$$

where k determines the shape of the elastica, q the initial point, and z is related with the length and point aggregation of the curve segment. We conclude that a general discrete elastica segment can be characterized by the seven parameters (3.97).

Remark 3.18 — Note that if we expand the sine and cosine functions in (3.96) and make use of (3.94), we obtain a recursive expression of ζ_n^Θ in terms of the Jacobi elliptic functions.

For the next section we need two extra results, and for them we introduce the following quantities: the projection of the curve γ_n onto the line $\mathrm{L}_\phi := \{{}^{\mathrm{t}}(\sin\phi, -\cos\phi)t \mid t \in \mathbb{R}\}$,

$$u_n := \left\langle \begin{pmatrix} \sin\phi \\ -\cos\phi \end{pmatrix}, \gamma_n \right\rangle, \tag{3.98}$$

and the turning angle of the curve measured from L_ϕ, denoted as $\Psi_n := \frac{\pi}{2} + \psi_n - \phi$, which satisfies that

$$\begin{cases} \cos\Psi_n = -\sin(\psi_n - \phi), \\ \sin\Psi_n = \cos(\psi_n - \phi). \end{cases} \tag{3.99}$$

Proposition 3.19 — *The discrete curvature κ_n is an affine function of the projection u_n, satisfying*

$$\kappa_n = \frac{\mu}{\Lambda} u_n + A, \tag{3.100}$$

where $\Lambda \in \mathbb{R}$ satisfies (3.65) and $A \in \mathbb{R}$ is a constant.

Proof. In the context of the proof of Proposition 3.12, after incorporating ϕ and putting $\epsilon = \mu h^2/4$, from (3.72) and (3.73) we obtain

$$\frac{\kappa_{n+1} - \kappa_n}{h} = -\frac{\mu}{\Lambda}\sin(\psi_n - \phi). \tag{3.101}$$

Then, noticing that $u_{n+1} - u_n = h\left\langle {}^{\mathrm{t}}(\sin\phi, -\cos\phi), T_n \right\rangle$, we have

$$\frac{u_{n+1} - u_n}{h} = -\sin(\psi_n - \phi). \tag{3.102}$$

Hence, by comparing equations (3.100) and (3.101), we conclude that there exists a constant $A \in \mathbb{R}$ such that, for all n,

$$\kappa_n = \frac{\mu}{\Lambda} u_n + A. \tag{3.103}$$

□

Remark 3.20 — Note that, by putting $\mu_1 = \mu\cos\phi$ and $\mu_2 = \mu\sin\phi$, equation (3.100) can be expressed as

$$\kappa_n = \frac{1}{\Lambda}(\mu_2 x_n - \mu_1 y_n) + A, \tag{3.104}$$

where $x_n, y_n \in \mathbb{R}$ are the two components of $\gamma_n = {}^{\mathrm{t}}(x_n, y_n)$.

Corollary 3.21 — *It holds that*

$$\sin\Psi_n = \frac{\mu}{2\Lambda}u_{n+1}u_n + A\frac{u_{n+1}+u_n}{2} + B, \tag{3.105}$$

where $B \in \mathbb{R}$ is a constant.

Proof. From the definition of u_n and Ψ_n, (3.98) and (3.99), respectively, we obtain

$$T_n = \mathrm{R}_\phi \begin{pmatrix} \sin\Psi_n \\ -\frac{u_{n+1}-u_n}{h} \end{pmatrix}, \qquad N_n = \mathrm{R}_\phi \begin{pmatrix} \frac{u_{n+1}-u_n}{h} \\ \sin\Psi_n \end{pmatrix}. \tag{3.106}$$

Then, putting this into the discrete Frenet formula,

$$\frac{T_n - T_{n-1}}{h} = \kappa_n \frac{N_n + N_{n-1}}{2}, \tag{3.107}$$

gives

$$\sin\Psi_n - \sin\Psi_{n-1} = \frac{1}{2}\left(\frac{\mu}{\Lambda}u_n + A\right)(u_{n+1} - u_{n-1}), \tag{3.108}$$

where we used (3.100). After expanding the right-hand side of the previous expression and then adding $\pm\frac{A}{2}u_n$, we conclude that there exists a constant $B \in \mathbb{R}$ such that, for all n,

$$\sin\Psi_n = \frac{\mu}{2\Lambda}u_{n+1}u_n + A\frac{u_{n+1}+u_n}{2} + B. \tag{3.109}$$

□

3.3.1 Fairing process methodology

Given a general discrete curve segment $\gamma_n \in \mathbb{R}^2$ $(n = 0, \ldots, N-1)$, we look for a discrete elastica $\zeta_n^\Theta \in \mathbb{R}^2$ that is the closest to γ_n in a L^2-distance sense. Namely, we seek to find Θ^* such that

$$\Theta^* = \arg\min_{\Theta\in U}\left\{\frac{1}{2}\sum_{n=0}^{N-1}\left\|\zeta_n^\Theta - \gamma_n\right\|^2\right\}, \tag{3.110}$$

with the admissible set U given by

$$U = \left\{(x_0, y_0, h, \phi, z, q, k) \in \mathbb{R}^7 \;\middle|\; \begin{array}{l}(x_0, y_0) \in \mathbb{R}^2, h > 0, \phi \in [0, 2\pi), \\ z, q \in \mathbb{R} \text{ and } k > 0\end{array}\right\}. \tag{3.111}$$

The non-convex optimization problem is solved using the Interior Point Optimizer (IPOPT) package, which for our purpose can be seen as a gradient descent-like

method for nonlinear optimizations [47]. For its implementation we need two objects: the gradient of the objective function,

$$\mathcal{L}(\Theta) := \sum_{n=0}^{N-1} \frac{1}{2} \left\| \zeta_n^\Theta - \gamma_n \right\|^2, \tag{3.112}$$

and an initial guess to start the optimization. The gradient of the objective function is computed as follows: From (3.112), we have

$$\frac{\partial}{\partial \Theta_i} \mathcal{L}(\Theta) = \sum_{n=0}^{N-1} \left\langle \zeta_n^\Theta - \gamma_n, \frac{\partial}{\partial \Theta_i} \zeta_n^\Theta \right\rangle, \qquad \Theta_i = x_0, y_0, h, \phi, z, q, k, \tag{3.113}$$

which is computed recursively from (3.96), using that

$$\frac{\partial}{\partial \Theta_i} \zeta_n^\Theta = \frac{\partial}{\partial \Theta_i} \zeta_{n-1}^\Theta + \begin{cases} 0, & \Theta_i = x_0, y_0, \\ T_n, & \Theta_i = h, \\ h \frac{\partial}{\partial \Theta_i} T_n, & \text{otherwise}, \end{cases} \tag{3.114}$$

with

$$\frac{\partial}{\partial \Theta_i} \zeta_0^\Theta = \begin{cases} {}^{\mathrm{t}}(1,0), & \Theta_i = x_0, \\ {}^{\mathrm{t}}(0,1), & \Theta_i = y_0, \\ {}^{\mathrm{t}}(0,0), & \text{otherwise}. \end{cases} \tag{3.115}$$

Next, from the properties of the trigonometric functions, we compute the gradient of the tangent by

$$\frac{\partial}{\partial \Theta_i} T_n = N_n \times \begin{cases} 1, & \Theta_i = \phi, \\ \mathcal{F}_n^{(i)}, & \Theta_i = z, q, k, \end{cases} \tag{3.116}$$

with

$$\mathcal{F}_n^{(i)} = \frac{1}{\cos\left(\frac{\theta_{n+1}-\phi}{2}\right)} \frac{\partial}{\partial \Theta_i} \sin\left(\frac{\theta_{n+1}-\phi}{2}\right) + \frac{1}{\cos\left(\frac{\theta_n-\phi}{2}\right)} \frac{\partial}{\partial \Theta_i} \sin\left(\frac{\theta_n-\phi}{2}\right), \tag{3.117}$$

or equivalently,

$$\mathcal{F}_n^{(i)} = -\frac{1}{\sin\left(\frac{\theta_{n+1}-\phi}{2}\right)} \frac{\partial}{\partial \Theta_i} \cos\left(\frac{\theta_{n+1}-\phi}{2}\right) - \frac{1}{\sin\left(\frac{\theta_n-\phi}{2}\right)} \frac{\partial}{\partial \Theta_i} \cos\left(\frac{\theta_n-\phi}{2}\right). \tag{3.118}$$

Finally, we use (3.95), (3.94) and the derivatives of the Jacobi elliptic functions with respect to their argument and module (cf. [27]) to obtain an explicit expression of (3.116), and this completes all the calculations required to obtain (3.113).

3.3.2 Initial guess

The IPOPT method needs a starting point $\bar{\Theta}$, which we refer as the **initial guess**. In this section, we describe the algorithm that we use to obtain the initial guess, which is a discrete analogue of the one provided in [6]. To estimate ϕ, z, q, and k we use some results from the smooth elastica. We use the following approximations: Using the parameterization (3.80) from Remark 3.13, equations (3.104) and (3.105) are expanded in terms of $\sqrt{\mu}h$ to give

$$\kappa_n = \mu_2 x_n - \mu_1 y_n + A + O(\mu h^2), \tag{3.119}$$

$$\sin \Psi_n = \frac{1}{2}\mu u_n^2 + A u_n + B + O(\mu h^2), \tag{3.120}$$

respectively. For the discrete curvature, consider the following: Solutions (3.52) and (3.51) can be written respectively as

[WI]

$$\kappa_n = \kappa_{\max} \operatorname{cn}(zn + q; k), \qquad \kappa_{\max} = \frac{2}{h}\frac{k \operatorname{sn}(z;k)}{\operatorname{dn}(z;k)}, \tag{3.121}$$

[NI]

$$\kappa_n = \kappa_{\max} \operatorname{dn}(k^{-1}(zn + q); k), \qquad \kappa_{\max} = \frac{2}{h}\frac{\operatorname{sn}(k^{-1}z;k)}{\operatorname{cn}(k^{-1}z;k)}. \tag{3.122}$$

From Remark 3.13 and Remark 3.15, we have $\alpha = 2 + \lambda h^2 + O(h^4)$, which is compatible with the parameterization $z = \sqrt{\mu}h + O(h^2)$ (see Remark 3.9). Hence, we obtain that $\kappa_{\max}$ satisfies

[WI]

$$\kappa_{\max} = 2k\sqrt{\mu} + O(\mu h^2), \tag{3.123}$$

[NI]

$$\kappa_{\max} = 2k^{-1}\sqrt{\mu} + O(\mu h^2). \tag{3.124}$$

For the parameter k we use the following: From (3.120), we note that u_n must be bounded from above and below, with the upper bound $u_{\max}$ being

$$u_{\max} = \frac{-A + \Delta}{\mu} + O(h^2), \qquad \Delta = \sqrt{A^2 - 2\mu(B-1)}. \tag{3.125}$$

Noticing that $u_{\max}$ occurs at the same instance than $\kappa_{\max}$, from (3.100) we get

$$\kappa_{\max} = \Delta + O(\mu h^2). \tag{3.126}$$

Hence, from (3.123) we obtain

[WI]

$$k = \frac{\Delta}{2\sqrt{\mu}} + O(\sqrt{\mu}h^2), \tag{3.127}$$

[NI]

$$k = \frac{2\sqrt{\mu}}{\Delta} + O(\sqrt{\mu}h^2). \tag{3.128}$$

Initial guess pseudo-algorithm

As the last part of this chapter, we present an algorithmic approach to obtain the initial guess

$$\bar{\Theta} = \left(\bar{x}_0, \bar{y}_0, \bar{h}, \bar{\phi}, \bar{z}, \bar{q}, \bar{k}\right), \tag{3.129}$$

for a given a discrete curve γ_n, $n = 0, \ldots, N-1$, with step size h. Firstly, we compute the following quantities. The turning angle,

$$\begin{pmatrix} \cos\psi_n \\ \sin\psi_n \end{pmatrix} = \frac{\gamma_{n+1} - \gamma_n}{h}, \qquad n = 0, \ldots, N-2, \tag{3.130}$$

and the discrete curvature,

$$\kappa_n = \frac{2}{h}\tan\frac{\psi_n - \psi_{n-1}}{2}, \qquad n = 1, \ldots, N-2. \tag{3.131}$$

❖ **Parameter $\boldsymbol{\phi}$** — We solve (3.119) in the least square sense,

$$(\bar{\mu}_1, \bar{\mu}_2, \bar{A}) = \underset{(\mu_1,\mu_2,A)}{\arg\min}\left\{\frac{1}{2}\sum_{n=1}^{N-2}(\kappa_n + \mu_1 y_n - \mu_2 x_n - A)^2\right\}. \tag{3.132}$$

Then, define $\bar{\mu} := \sqrt{\bar{\mu}_1^2 + \bar{\mu}_2^2}$ and set $\bar{\phi}$ such that

$$\cos\bar{\phi} = \frac{\bar{\mu}_1}{\bar{\mu}}, \qquad \sin\bar{\phi} = \frac{\bar{\mu}_2}{\bar{\mu}}. \tag{3.133}$$

❖ **Parameter $\boldsymbol{k}$** — Using $\bar{\mu}$ and $\bar{A}$, we solve (3.120) in the least square sense,

$$\bar{B} = \underset{B}{\arg\min}\left\{\frac{1}{2}\sum_{n=0}^{N-2}\left(\sin\Psi_n - \frac{1}{2}\bar{\mu}u_n^2 - \bar{A}u_n - B\right)^2\right\}. \tag{3.134}$$

Then, from (3.127), if $\bar{B} < \frac{\bar{A}^2}{2\bar{\mu}} - 1$ we are in case of the Elastica with inflections,

[WI]

$$\bar{k} = 2\left(\frac{\bar{A}^2}{\bar{\mu}} - 2(\bar{B}-1)\right)^{-1/2}, \tag{3.135}$$

otherwise ($\bar{B} \geq \frac{\bar{A}^2}{2\bar{\mu}} - 1$) we are in case without inflections,

[NI]

$$\bar{k} = \frac{1}{2}\left(\frac{\bar{A}^2}{\bar{\mu}} - 2(\bar{B}-1)\right)^{1/2}. \tag{3.136}$$

❖ **Parameter q, z** — For simplicity, let us denote $s_n := zn + q$. Define $m \in \mathbb{N}$ as the number of segments in which the function u_n is monotone. We counted m manually, although it could also be estimated by, for example,

[WI]

$$\bar{m} = \left\lceil (N-1)h\,\frac{\sqrt{\bar{\mu}}}{2K(\bar{k})} \right\rceil (+1), \tag{3.137}$$

[NI]

$$\bar{m} = \left\lceil (N-1)h\,\frac{\sqrt{\bar{\mu}}}{K(\bar{k})} \right\rceil (+1), \tag{3.138}$$

where K is the complete elliptic integral of the first kind, and the term in brackets $(+1)$ is added only if both u_0 and u_{N-1} are simultaneously increasing or decreasing. Then, we simply invert the Jacobi elliptic function at the endpoints $n = 0$ and $n = N-1$ to obtain q and z, using that $\mathrm{sn}^{-1} = F \circ \arcsin$, $\mathrm{cn}^{-1} = F \circ \arccos$, where F is the elliptic integral of the first kind. Concretely, from (3.121) and (3.123), we have the following:

[WI]

$$\mathrm{cn}(zn + q; \bar{k}) = \frac{\bar{\mu}u_n + \bar{A}}{2\bar{k}\sqrt{\bar{\mu}}} \equiv U_n. \tag{3.139}$$

Hence,

– If u_n is decreasing on the first segment:

$$s_0 = F(\arccos U_0; \bar{k}), \tag{3.140}$$

and

$$s_{N-1} = \begin{cases} 2(m-1)K(\bar{k}) + F(\arccos U_{N-1}; \bar{k}), & m \text{ is odd}, \\ 2mK(\bar{k}) - F(\arccos U_{N-1}; \bar{k}), & m \text{ is even}. \end{cases} \tag{3.141}$$

– If u_n is increasing on the first segment:

$$s_0 = 4K(\bar{k}) - F(\arccos U_0; \bar{k}), \tag{3.142}$$

and

$$s_{N-1} = \begin{cases} 2(m+1)K(\bar{k}) - F(\arccos U_{N-1}; \bar{k}), & m \text{ is odd}, \\ 2mK(\bar{k}) + F(\arccos U_{N-1}; \bar{k}, & m \text{ is even}. \end{cases} \tag{3.143}$$

[NI]

$$\mathrm{dn}(\bar{k}^{-1} s_n; \bar{k}) = \frac{\bar{\mu} u_n + \bar{A}}{2\bar{k}^{-1}\sqrt{\bar{\mu}}}, \tag{3.144}$$

which can be rewritten as

$$\mathrm{sn}(\bar{k}^{-1} s_n; \bar{k}) = \bar{k}^{-1} \sqrt{1 - \left(\frac{\bar{\mu} u_n + \bar{A}}{2\bar{k}^{-1}\sqrt{\bar{\mu}}} \right)^2} \equiv U_n. \tag{3.145}$$

Hence,

– If u_n is decreasing on the first segment:

$$s_0 = \bar{k} F(\arcsin U_0; \bar{k}), \tag{3.146}$$

and

$$s_{N-1} = \begin{cases} (m-1)\bar{k}K(\bar{k}) + \bar{k}F(\arcsin U_{N-1}; \bar{k}), & m \text{ is odd}, \\ m\bar{k}K(\bar{k}) - \bar{k}F(\arcsin U_{N-1}; \bar{k}), & m \text{ is even}. \end{cases} \tag{3.147}$$

– If u_n is increasing on the first segment:

$$s_0 = 2\bar{k}K(\bar{k}) - \bar{k}F(\arcsin U_0; \bar{k}), \tag{3.148}$$

and

$$s_{N-1} = \begin{cases} (m+1)\bar{k}K(\bar{k}) - \bar{k}F(\arcsin U_{N-1}; \bar{k}), & m \text{ is odd}, \\ m\bar{k}K(\bar{k}) + \bar{k}F(\arcsin U_{N-1}; \bar{k}), & m \text{ is even}. \end{cases} \tag{3.149}$$

Finally, we set

$$\bar{q} = s_0, \qquad \bar{z} = \frac{1}{N-1}(s_{N-1} - s_0). \tag{3.150}$$

❖ **Parameter x_0, y_0, h** — From the previous steps, using all the recovered parameters, we construct a discrete elastica segment that starts at the origin with parameters $\check{\Theta} = (0, 0, h, \bar{\phi}, \bar{z}, \bar{q}, \bar{k})$. Then,

$$\begin{pmatrix} \bar{x}_0 \\ \bar{y}_0 \end{pmatrix} = \underset{{}^{\mathrm{t}}(x_0, y_0)}{\arg\min} \left\{ \frac{1}{2} \sum_{n=0}^{N-1} \left(\gamma_n - \zeta_n^{\check{\Theta}} \right)^2 \right\}. \tag{3.151}$$

For the step size, we just set $\bar{h} = h$.

Figure 3.3 illustrates typical examples of the fairing method, where we used the above algorithm to obtain the initial guess.

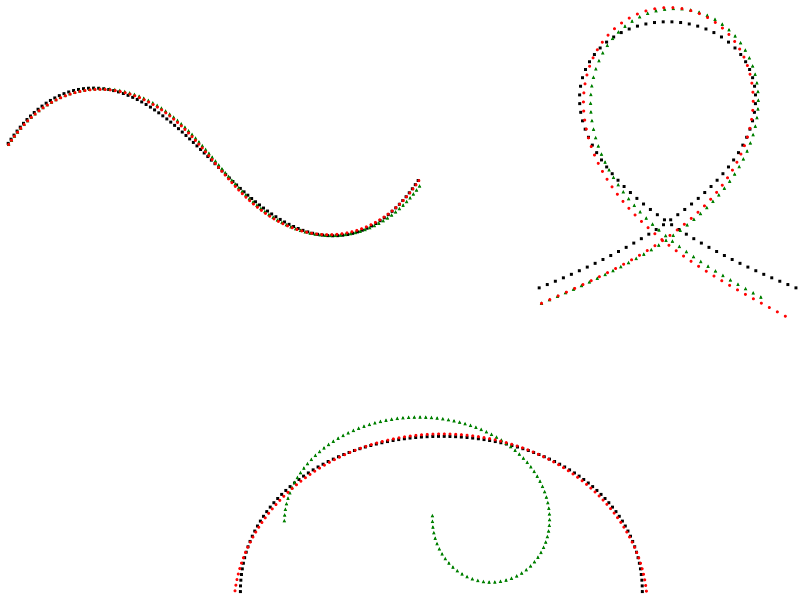

Figure 3.3: Typical examples of the fairing of discrete planar curves to discrete Euler's elasticae. Black squares are the input curve, green triangles are the initial guess, and red circles are the output elasticae.

Chapter 4

Fairing to Log-aesthetic curves

This chapter addresses the Log-aesthetic curve. In Section 4.1, we present the basic definitions and show a result that helps characterize the family of Log-aesthetic curves via similarity transformations. In Section 4.2, in a similar manner than in the previous chapter, we present an algorithmic approach to fair planar curves to Log-aesthetic curves. Part of the content of this chapter is included in [14].

4.1 Log-aesthetic curve

In [15], T. Harada et al. presented a quantitative and qualitative study of planar curves sampled from the keylines of a car and suggested that, for aesthetically pleasing curves, the frequency histogram of the radius of curvature follows a piecewise linear relation in a log-log scale. In [36, 50], by considering an analytic formulation of the work by T. Harada et al., it is shown that such curves satisfy

$$\log\left(\frac{\mathrm{d}s}{\mathrm{d}R}\right) = \alpha R - \log A, \tag{4.1}$$

for some $\alpha \in \mathbb{R}$ and $A > 0$, where $R = \log \rho$. These curves will later be coined as **log-aesthetic curves** (or simply referred to as LAC), and (4.1) is usually given as the defining equation. In this thesis, we consider the following, equivalent, definition:

Definition 4.1 (Log-aesthetic curve) **—** An arc length parameterized curve $\gamma(s)$ with a strictly monotonic radius of curvature is called a *log-aesthetic curve (LAC)* if its curvature satisfies

$$\kappa\kappa'' - (\alpha + 1)(\kappa')^2 = 0, \tag{4.2}$$

for some constant $\alpha \in \mathbb{R}$.

Remark 4.2 — Assuming that functions are well-behaved, we have $\frac{\mathrm{d}s}{\mathrm{d}R} = \rho/\rho'$, then (4.1) is rewritten as

$$\rho'\rho^{(\alpha-1)} = A, \tag{4.3}$$

and by taking the derivative of (4.3), we obtain

$$\rho\rho'' + (\alpha - 1)(\rho')^2 = 0, \tag{4.4}$$

which is rewritten in terms of $\kappa = \rho^{-1}$ to give (4.2).

Let us see that the parameter α of a given LAC is invariant under the similarity transformations and reflections. Firstly, note that because the curvature of a planar curve is invariant under the Euclidean transformations, we only check the invariance under scale transformations and the reflections over the diagonal $\{(x,x) \in \mathbb{R}^2 | x \in \mathbb{R}\}$. For scale transformations, consider the arc length parameterized LAC $\gamma(s)$ satisfying (4.2), for some $\alpha \in \mathbb{R}$, and define $\tilde{\gamma}(\tilde{s}) := S\gamma(\tilde{s}/S)$, where $S > 0$. Then $\tilde{\kappa}(\tilde{s})$, the curvature of $\tilde{\gamma}(\tilde{s})$, is given by $\tilde{\kappa}(\tilde{s}) = S^{-1}\kappa(\tilde{s}/S)$ and it is easy to see that it satisfies (4.2). For the reflections over the diagonal, note that interchanging the $x-$ and $y-$component of the curve is equivalent to changing the sign of the curvature, and (4.2) is invariant under that change.

The fundamental theorem of planar curves states that an arc length parameterized planar curve is uniquely determined by its curvature up to Euclidean transformations. In addition, the curvature of an LAC determined by (4.2) has two arbitrary parameters. In view of this, we introduce the *basic LAC* by fixing this freedom and show that one can recover a general LAC by applying similarity transformations and shifting the arc length parameter.

Definition 4.3 (Basic LAC) **—** Let $\xi^\alpha(s)$ be an LAC defined over an open interval $I \subset \mathbb{R}$, such that $\{0\} \in I$, and satisfying

$$\begin{cases} \kappa'(s) = -(\kappa(s))^{(\alpha+1)} < 0, & \forall s \in I, \\ \kappa(0) = 1, \\ \psi(0) = 0, \\ \xi^\alpha(0) = 0. \end{cases} \tag{4.5}$$

We call $\xi^\alpha(s)$ a *basic LAC*.

Let us see a more explicit expression for the basic LAC and its related quantities. In what follows, we use the sub-index ξ^α, as for example κ_{ξ^α}, to denote those quantities associated with their respective basic LAC. Taking the initial condition into consideration, the explicit form of the curvature is given by

$$\kappa_{\xi^\alpha}(s) = \begin{cases} \exp(-s), & \alpha = 0, \\ (1 + \alpha s)^{-1/\alpha}, & \alpha \neq 0. \end{cases} \tag{4.6}$$

Then, the turning angle is obtained from the curvature by $(\psi_{\xi^\alpha})' = \kappa_{\xi^\alpha}$,

$$\psi_{\xi^\alpha}(s) = \begin{cases} 1 - \exp(-s), & \alpha = 0, \\ \log(s+1), & \alpha = 1, \\ \frac{(1+\alpha s)^{\frac{\alpha-1}{\alpha}} - 1}{\alpha - 1}, & \alpha \neq 0, 1. \end{cases} \tag{4.7}$$

Although it is not used in this thesis, we note that the position vector can be expressed in terms of the incomplete gamma function, see for example [51]. For simplicity we consider the case in which $1 + \alpha s > 0$. In this case, the maximal interval $I_\alpha \subset \mathbb{R}$ on which the basic LAC can be defined is

$$I_\alpha = \begin{cases} (-\infty, -1/\alpha), & \alpha < 0, \\ (-\infty, \infty), & \alpha = 0, \\ (-1/\alpha, \infty), & \alpha > 0, \end{cases} \tag{4.8}$$

and we assume that all basic LAC are defined over I_α. Finally, note that the image of κ_{ξ^α} is $\kappa_{\xi^\alpha}[I_\alpha] = (0, \infty)$.

Proposition 4.4 — *Any LAC with $\alpha \neq 1$ and positive and decreasing curvature can be expressed as a basic LAC after applying similarity transformations and shifting the arc length parameter. In particular, if $\gamma(s)$, $s \in [0, L]$, is an LAC of length L, there exists a unique $\gamma_0 \in \mathbb{R}^2$, $\phi \in [0, 2\pi)$, $S \in \mathbb{R}\backslash\{0\}$, and $s_0 \in \mathbb{R}$, such that*

$$\gamma(s) = \gamma_0 + S\,\mathrm{R}_\phi\,\xi^\alpha(s/S + s_0), \qquad s \in [0, L], \tag{4.9}$$

where $\xi^\alpha(s)$ is a basic LAC of length L/S.

Proof. For a given LAC $\gamma(s)$, $s \in [0, L]$ with $\alpha \neq 1$ and positive and decreasing curvature, we know that its curvature satisfies (4.2), which can be integrated once to obtain

$$\kappa'(s) = -A(\kappa(s))^{(\alpha+1)}, \tag{4.10}$$

for some $A > 0$. Next, consider the curve $\bar{\gamma}(\bar{s}) := S^{-1}\gamma(\bar{s}S)$, $\bar{s} \in [0, L/S]$, and set $S = A^{1/(\alpha-1)}$. Note that the curvature of $\bar{\gamma}$ satisfies

$$\begin{cases} \bar{\kappa}'(\bar{s}) = -(\bar{\kappa}(\bar{s}))^{(\alpha+1)}, \\ \bar{\kappa}(0) = A^{1/(\alpha-1)}\kappa(0), \end{cases} \tag{4.11}$$

which can be integrated to obtain

$$\bar{\kappa}(\bar{s}) = \begin{cases} \exp(-(\bar{s} - \log\bar{\kappa}(0))), & \alpha = 0, \\ \left[1 + \alpha\left(\bar{s} + \frac{(\bar{\kappa}(0))^{-\alpha} - 1}{\alpha}\right)\right]^{-1/\alpha}, & \alpha \neq 0. \end{cases} \tag{4.12}$$

By comparing $\bar{\kappa}$ with κ_{ξ^α} in (4.6), there exists a unique $s_0 \in \mathbb{R}$ such that $\bar{\kappa}(\bar{s}) = \kappa_{\xi^\alpha}(\bar{s} + s_0)$. From the fundamental theorem of planar curves, it follows that the curves $\bar{\gamma}$ and ξ^α are congruent up to rigid transformations, i.e.

$$\bar{\gamma}(\bar{s}) = \bar{\gamma}_0 + \mathrm{R}_\phi\, \xi^\alpha(\bar{s} + s_0), \qquad \bar{s} \in [0, L/S], \tag{4.13}$$

for some $\bar{\gamma}_0 \in \mathbb{R}^2$ and $\phi \in [0, 2\pi)$. Finally, we use that $\gamma(s) = S\bar{\gamma}(s/S)$ to obtain (4.9) with $\gamma_0 := S\bar{\gamma}_0$. □

Remark 4.5 — In the proof of Proposition 4.4, the scale transformation is used to change the value of A, in (4.10), without changing the value of α. However, in the case of $\alpha = 1$ this technique cannot be exploited. Because, the case of $\alpha = 1$ corresponds to the logarithmic spiral, which is a self-similar curve. In particular, the value of A for a given logarithmic spiral is invariant under scale transformations, thus the technique used in Proposition 4.4 cannot be used to recover the entire family of LAC with $\alpha = 1$.

Remark 4.6 — Let X be the reflection of $\mathbb{R}^2$ defined by the map $(x, y) \mapsto (y, x)$. If $\gamma(s)$, $s \in [0, L]$, is an LAC, then also are

$$\begin{cases} \gamma^{(1)}(s) := \gamma(L - s), \\ \gamma^{(2)}(s) := X\gamma(s), \\ \gamma^{(3)}(s) := X\gamma(L - s). \end{cases} \tag{4.14}$$

Moreover, their respective curvatures satisfy

$$\begin{cases} \kappa^{(1)}(s) = -\kappa(L - s), \\ \kappa^{(2)}(s) = -\kappa(s), \\ \kappa^{(3)}(s) = \kappa(L - s), \end{cases} \tag{4.15}$$

which allow us to use Proposition 4.4 in those cases in which the curvature is not positive and decreasing, by applying one of the transformations (4.14).

4.1.1 Recovering the parameters of an LAC segment

We focus our attention on the problem of finding the parameters that uniquely identify a given LAC segment. We proceed in three steps, in which we solve several linear equations in the least-squares sense, with the objective of constructing an algorithm that can be applied to general curves. Before describing the method, we make use of the following remarks: In view of Remark 4.5 we omit the case

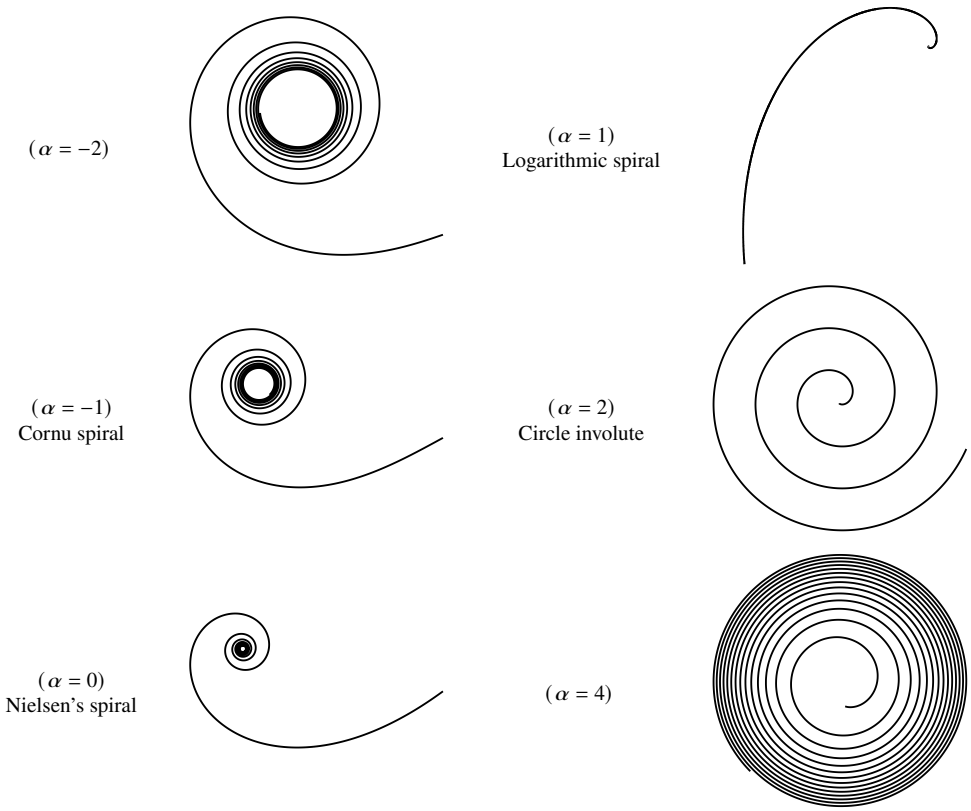

Figure 4.1: Typical examples of log-aesthetic curves.

$\alpha = 1$, and for simplicity in the formulation of this method we further omit the case $\alpha = 0$. Removing these values does not hinder the quality of the algorithm, because they are only single points on the real line. At last, given an LAC segment $\gamma(s)$, $s \in [0, L]$, by possibly applying one of the transformations (4.14), we assume that its curvature is positive and decreasing. Then, from Proposition 4.4, it follows that there exists a set of parameters $\{x_0, y_0, S, \phi, l, s_0, \alpha\}$ such that

$$\gamma(s) = \begin{pmatrix} x_0 \\ y_0 \end{pmatrix} + S\,\mathrm{R}_\phi\,\xi^\alpha(s/S + s_0), \qquad s \in [0, lS], \tag{4.16}$$

which implies, by definition of the curvature function, that

$$\kappa(s) = S^{-1}\kappa_{\xi^\alpha}(s/S + s_0). \tag{4.17}$$

Let $R = -\log\kappa$ and $R_{\xi^\alpha} = -\log\kappa_{\xi^\alpha}$, then

$$R(s) = \log S + R_{\xi^\alpha}(s/S + s_0). \tag{4.18}$$

Finally, from the differential equation (4.5) we have that $\log(R'_{\xi^\alpha}) + \alpha R_{\xi^\alpha} = 0$; hence, from (4.18), we obtain

$$\log(R') + \alpha R = (\alpha - 1)\log S. \tag{4.19}$$

Step 1 — Let $c_1 := \alpha$ and $c_0 := (\alpha - 1)\log S$. Then, from (4.19), in the least squares sense we have

$$(c_0, c_1) = \underset{(\bar{c}_0, \bar{c}_1)}{\arg\min} \left\{ \frac{1}{2} \int_0^L (\log(R') + \bar{c}_1 R - \bar{c}_0)^2 \, \mathrm{d}s \right\}, \tag{4.20}$$

which leads to

$$c_1 = \frac{L \int_0^L R \log(R') \, \mathrm{d}s - \int_0^L R \, \mathrm{d}s \int_0^L \log(R') \, \mathrm{d}s}{(\int_0^L R \, \mathrm{d}s)^2 - L \int_0^L R^2 \, \mathrm{d}s}, \tag{4.21}$$

and

$$c_0 = \frac{1}{L} \int_0^L (\log(R') + c_1 R) \, \mathrm{d}s. \tag{4.22}$$

Then, $\alpha = c_1$ and $S = \exp(c_0/(c_1 - 1))$.

Step 2 — From (4.6) and (4.17), we have that $\kappa(s) = S^{-1}(1 + \alpha(s/S + s_0))^{-1/\alpha}$, which allows us to isolate the parameter s_0 as

$$s_0 = \frac{(S\kappa(s))^{-\alpha}}{\alpha} - \frac{1}{\alpha} - \frac{s}{S}. \tag{4.23}$$

Then,

$$s_0 := \underset{\bar{s}_0}{\arg\min} \left\{ \frac{1}{2} \int_0^L \left(\frac{1}{\alpha S^\alpha \kappa(s)^\alpha} - \frac{1}{\alpha} - \frac{s}{S} - \bar{s}_0 \right)^2 \mathrm{d}s \right\} \tag{4.24}$$

gives

$$s_0 = \frac{1}{\alpha L S^\alpha} \int_0^L (\kappa(s))^{-\alpha} \, \mathrm{d}s - \frac{1}{\alpha} - \frac{1}{LS} \int_0^L s \, \mathrm{d}s. \tag{4.25}$$

Similarly, we compute $s_{\text{end}} := L/S + s_0$ from $\kappa^{(3)}(s) = \kappa(L - s) = S^{-1}(1 + \alpha(s_{\text{end}} - s/S))^{-1/\alpha}$. In the least squares sense, we obtain

$$s_{\text{end}} = \frac{1}{\alpha L S^\alpha} \int_0^L (\kappa(L - s))^{-\alpha} \, \mathrm{d}s - \frac{1}{\alpha} + \frac{1}{LS} \int_0^L s \, \mathrm{d}s, \tag{4.26}$$

Hence,

$$l = s_{\text{end}} - s_0 = L/S. \tag{4.27}$$

Step 3 — At this point, it remains to find the rotation and translation parameters. For the former, note that the angle function of γ and ξ^α differ only by a constant ϕ, as

$$\psi(s) = \phi + \psi_{\xi^\alpha}(s/S + s_0). \tag{4.28}$$

Thus, in the least squares sense we obtain

$$\phi = \frac{1}{L}\int_0^L (\psi(s) - \psi_{\xi^\alpha}(s/S + s_0))\,\mathrm{d}s. \tag{4.29}$$

Finally, for the translation (x_0, y_0) we solve (4.9) in the least squares sense,

$$\begin{pmatrix} x_0 \\ y_0 \end{pmatrix} = \frac{1}{L}\int_0^L \left(\gamma(s) - S\,\mathrm{R}_\phi\,\xi^\alpha(s/S + s_0)\right)\mathrm{d}s. \tag{4.30}$$

4.2 Fairing of planar curves

In this section, we consider the case where a general planar curve segment is given and we want to find an LAC segment that is the closest in a L^2-distance sense. For all the applications that we have in mind, the input data is regarded as a discrete curve, thus we must consider a discretization of the LAC and of the previous results.

General log-aesthetic curve segment

From Proposition 4.4, we know that a general LAC segment $\xi(s)$, $s \in [0, L]$, after a possible change of parameterization or a reflection (see Remark 4.6), can be expressed as

$$\xi(s) = \begin{pmatrix} x_0 \\ y_0 \end{pmatrix} + S\,\mathrm{R}_\phi\,\xi^\alpha(s/S + s_0), \qquad s \in [0, L], \tag{4.31}$$

where ξ^α is a basic LAC with total length $l := L/S$. Furthermore, $\xi(s)$ is also rewritten as

$$\xi(s) = \begin{pmatrix} x_0 \\ y_0 \end{pmatrix} + \int_0^s \begin{pmatrix} \cos(\psi_{\xi^\alpha}(t/S + s_0) + \phi) \\ \sin(\psi_{\xi^\alpha}(t/S + s_0) + \phi) \end{pmatrix}\mathrm{d}t, \qquad s \in [0, L], \tag{4.32}$$

where ψ_{ξ^α} is given by (4.7). From now on, let us consider a discretization of (4.32). Let $N \in \mathbb{N}$, and define

$$\begin{cases} h := \frac{L}{N-1}, \\ z := \frac{L}{S(N-1)} = \frac{l}{N-1}, \\ q := s_0, \end{cases} \tag{4.33}$$

and the discrete curve $\xi_n^\Theta \in \mathbb{R}^2$, $n = 0, \dots, N-1$, such that

$$\begin{cases} \xi_n^\Theta = \xi_{n-1}^\Theta + h\begin{pmatrix}\cos(\psi_{\xi^\alpha}(zn+q)+\phi)\\ \sin(\psi_{\xi^\alpha}(zn+q)+\phi)\end{pmatrix}, & n = 1, \dots, N-1, \\ \xi_0^\Theta = \begin{pmatrix}x_0\\ y_0\end{pmatrix}, \end{cases} \tag{4.34}$$

where we introduced the notation ξ_n^Θ for the discrete curve that depends on the parameters

$$\Theta := (x_0, y_0, h, \phi, z, q, \alpha). \tag{4.35}$$

Note that, the recursive expression (4.34) gives an approximation of $\xi(s)$ of second order, in the sense that

$$\begin{cases} \xi(s) &= \xi_n^\Theta + O(h^2), \\ T(s) &= T_n, \\ \psi(s) &= \psi_n, \\ \kappa(s) &= \kappa_n + O(h^2), \end{cases} \tag{4.36}$$

where $s = hn$, and the discrete objects are computed from their definition (see Section 2.2). We conclude that a general LAC segment can be approximated by ξ_n^Θ which depends on the seven parameters (4.35).

Remark 4.7 — From (4.34) and (4.36), note that the discrete turning angle of ξ_n^Θ is given by $\psi_n = \psi_{\xi^\alpha}(zn+q) + \phi$; hence,

$$\psi_n = \frac{(1+\alpha(zn+q))^{\frac{\alpha-1}{\alpha}} - 1}{\alpha - 1} + \phi. \tag{4.37}$$

4.2.1 Fairing process methodology

The input data for the fairing process is assumed to be a list of N two-dimensional points, regarded as a discrete curve with constant step size,

$$\gamma_n = \begin{pmatrix}x_n\\ y_n\end{pmatrix}, \qquad n = 0, \dots, N-1. \tag{4.38}$$

Given γ_n, we look for an LAC segment $\xi_n^\Theta \in \mathbb{R}^2$ that is the closest to γ_n, in the L^2-distance sense. Namely, we seek to find a set of parameters Θ^* such that

$$\Theta^* = \underset{\Theta \in U}{\arg\min}\left\{ \frac{1}{2}\sum_{n=0}^{N-1} \left\| \xi_n^\Theta - \gamma_n \right\|^2 \right\}, \tag{4.39}$$

with the admissible set U given by

$$U = \left\{ (x_0, y_0, \phi, h, z, q, \alpha) \in \mathbb{R}^7 \;\middle|\; \begin{array}{l} (x_0, y_0) \in \mathbb{R}^2, h > 0, \phi \in [0, 2\pi), \\ z > 0, q \in I_\alpha \text{ and } \alpha \in \mathbb{R}\backslash\{0, 1\} \end{array} \right\}. \tag{4.40}$$

The optimization problem is solved using the Interior Point Optimizer (IPOPT) package [47], so we need the gradient of the objective function and an initial guess to start the optimization. Following our previous explanation in Section 3.3.1 (for the Euler's elastica), let us compute the gradient of

$$\mathcal{L}(\Theta) := \frac{1}{2} \sum_{n=0}^{N-1} \left\| \xi_n^\Theta - \gamma_n \right\|^2. \tag{4.41}$$

We have,

$$\frac{\partial}{\partial \Theta_i} \mathcal{L}(\Theta) = \sum_{n=0}^{N-1} \left\langle \xi_n^\Theta - \gamma_n, \frac{\partial}{\partial \Theta_i} \xi_n^\Theta \right\rangle, \qquad \Theta_i = x_0, y_0, \phi, h, z, q, \alpha, \tag{4.42}$$

which is computed recursively from equation (4.34), using that

$$\frac{\partial}{\partial \Theta_i} \xi_n^\Theta = \frac{\partial}{\partial \Theta_i} \xi_{n-1}^\Theta + \begin{cases} 0, & \Theta_i = x_0, y_0, \\ T_n, & \Theta_i = h, \\ h \frac{\partial}{\partial \Theta_i} T_n, & \text{otherwise}, \end{cases} \tag{4.43}$$

with

$$\frac{\partial}{\partial \Theta_i} \xi_0^\Theta = \begin{cases} {}^{\mathrm{t}}(1, 0), & \Theta_i = x_0, \\ {}^{\mathrm{t}}(0, 1), & \Theta_i = y_0, \\ {}^{\mathrm{t}}(0, 0), & \text{otherwise}, \end{cases} \tag{4.44}$$

where T_n is computed as

$$T_n := \begin{pmatrix} \cos(\psi_{\xi^\alpha}(zn + q) + \phi) \\ \sin(\psi_{\xi^\alpha}(zn + q) + \phi) \end{pmatrix}. \tag{4.45}$$

Then, using that $(\psi_{\xi^\alpha})' = \kappa_{\xi^\alpha}$, we obtain the gradient of T_n by

$$\frac{\partial}{\partial \Theta_i} T_n = \mathrm{R}_{\pi/2}\, T_n \times \begin{cases} 1, & \Theta_i = \phi, \\ \kappa_{\xi^\alpha}(zn + q), & \Theta_i = q, \\ n\kappa_{\xi^\alpha}(zn + q), & \Theta_i = z, \\ \frac{\partial}{\partial \alpha} \psi_{\xi^\alpha}(zn + q), & \Theta_i = \alpha, \end{cases} \tag{4.46}$$

with

$$\frac{\partial}{\partial\alpha}\psi_{\xi^\alpha}(s) = \frac{1}{(\alpha-1)^2} + \frac{(1+s\alpha)^{-\frac{1}{\alpha}}\Big((\alpha-1)(1+s\alpha)\log(1+s\alpha) - \alpha\big(\alpha+2s\alpha-s\big)\Big)}{\alpha^2(\alpha-1)^2}, \quad (4.47)$$

which is obtained by direct computation from (4.7).

4.2.2 Initial guess

In this section, in analogy to Section 3.3.2, we describe the algorithm that we use to obtain the initial guess. As it was mentioned in the previous section, we regard the input data as a discrete curve; hence, we use a discrete analogue to the three steps described in Section 4.1.1.

Initial guess pseudo-algorithm:

We present an algorithmic approach to obtain the initial guess

$$\bar{\Theta} = \big(\bar{x}_0, \bar{y}_0, \bar{h}, \bar{\phi}, \bar{z}, \bar{q}, \bar{\alpha}\big), \quad (4.48)$$

for a given a discrete curve γ_n, $n = 0, \dots, N-1$, with step size h. Firstly, we compute the following quantities: From the tangent vector,

$$T_n = \frac{\gamma_{n+1} - \gamma_n}{h}, \qquad n = 0, \dots, N-2, \quad (4.49)$$

and using that the sine and cosine of the deflection angle satisfies that $\sin K_n = \det(T_{n-1}, T_n)$ and $\cos K_n = \langle T_{n-1}, T_n\rangle$, we compute the turning angle by

$$\begin{cases} \psi_n = \psi_{n-1} + \arctan(\det(T_{n-1}, T_n)/\langle T_{n-1}, T_n\rangle), & n = 1, \dots, N-2, \\ \psi_0 = \arctan\big(\det\big({}^{\mathrm{t}}(1,0), T_0\big)/\big\langle {}^{\mathrm{t}}(1,0), T_0\big\rangle\big), \end{cases} \quad (4.50)$$

and the curvature by

$$\kappa_n = \frac{2}{h}\frac{\det(T_{n-1}, T_n)}{1 + \langle T_{n-1}, T_n\rangle}, \qquad n = 1, \dots, N-2. \quad (4.51)$$

Then, let us define the logarithm of the radius of curvature by

$$R_n = -\log\kappa_n, \qquad n = 1, \dots, N-2, \quad (4.52)$$

and its discrete derivative by

$$\Delta R_n = -\frac{\kappa_{n+1} - \kappa_n}{\kappa_n}, \qquad n = 1, \dots, N-3. \tag{4.53}$$

❖ **Parameter α** — Following Step 1, we solve

$$(\bar{c}_0, \bar{c}_1) = \underset{(c_0,c_1)}{\arg\min} \left\{ \frac{1}{2} \sum_{n=1}^{N-3} (\log(\Delta R_n/h) + c_1 R_n - c_0)^2 h \right\}. \tag{4.54}$$

Then, using that $\bar{\alpha} = c_0$ and $\bar{S} = \exp(c_0/(c_1 - 1))$, we obtain

$$\bar{\alpha} = \frac{(N-3)\sum_{n=1}^{N-3} R_n \log \Delta R_n - \sum_{n=1}^{N-3} R_n \sum_{n=1}^{N-3} \log \Delta R_n}{\left(\sum_{n=1}^{N-3} R_n\right)^2 - (N-3)\sum_{n=1}^{N-3} R_n^2}, \tag{4.55}$$

and

$$\bar{S} = h^{\frac{1}{1-\bar{\alpha}}} \exp\left(\frac{1}{(\bar{\alpha}-1)(N-3)} \sum_{n=1}^{N-3} (\log \Delta R_n + \bar{\alpha} R_n) \right). \tag{4.56}$$

❖ **Parameter q, z** — From Step 2, and using that $q = s_0$, and $\bar{z} = \bar{l}/(N-1)$, we obtain

$$\bar{q} = \frac{1}{\bar{\alpha}(N-2)\bar{S}^{\bar{\alpha}}} \sum_{n=1}^{N-2} (\kappa_n)^{-\bar{\alpha}} - \frac{1}{\bar{\alpha}} - \frac{(N-1)h}{2\bar{S}}, \tag{4.57}$$

and

$$\bar{z} = \frac{(N-1)h}{\bar{S}}. \tag{4.58}$$

❖ **Parameter ϕ, x_0, y_0, h** — Let $\xi_n^{\breve{\Theta}}$, $n = 0, \dots, N-1$, be the discrete curve computed as in (4.34) with $\breve{\Theta} = (0, 0, h, 0, \bar{z}, \bar{q}, \bar{\alpha})$. Then, its turning angle is $\psi_{\xi^{\bar{\alpha}}}(\bar{z}n + \bar{s}_0)$; hence, following Step 3, we obtain

$$\bar{\phi} = \frac{1}{N-1} \sum_{n=0}^{N-2} (\psi_n - \psi_{\xi^{\bar{\alpha}}}(\bar{z}n + \bar{q})), \tag{4.59}$$

and

$$\begin{pmatrix} \bar{x}_0 \\ \bar{y}_0 \end{pmatrix} = \frac{1}{N} \sum_{n=0}^{N-1} \left(\gamma_n - \mathrm{R}_{\bar{\phi}}\, \xi_n^{\breve{\Theta}} \right). \tag{4.60}$$

Finally, we set $\bar{h} = h$.

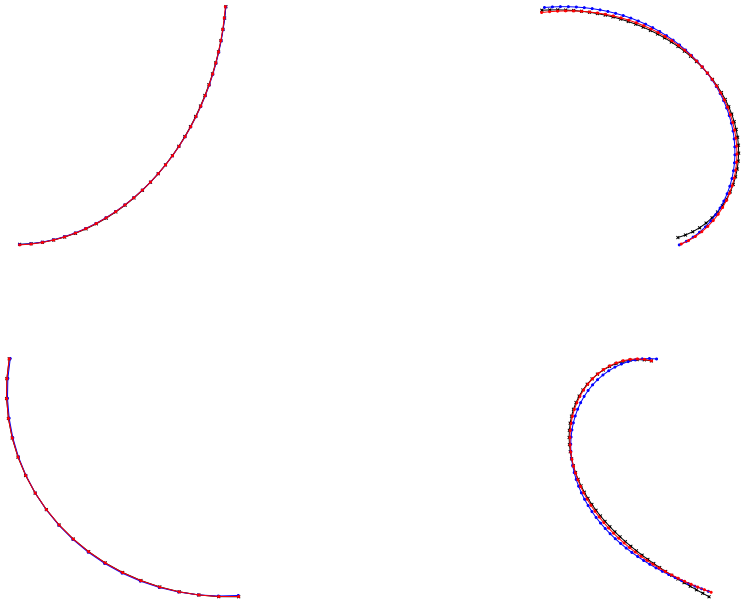

Figure 4.2: Examples of discrete curves approximated by LAC. Black curves are the input curves, blue curves are the first guesses and the red curves are the final outputs of the IPOPT program. The parameter α obtained is: 1.310 (upper-left), 0.547 (upper-right), -9.254 (bottom-left), and -1.033 (bottom-right).

As a first test for this algorithm, we used synthetic data: discrete curves with constant step size based on Bézier curves. These curves were split in segments with sign preserving monotonic curvature. Then, we faired each segment to an LAC, using the previous algorithm to compute the initial guess. Some examples are shown in Figure 4.2. In the next section we apply this method to real data.

Chapter 5

Applications

In this chapter, we present an example of usage of the fairing algorithms described in Section 3.3 and Section 4.2, for the Euler's elastica and log-aesthetic curve, respectively. In both cases, we seek to characterize the keylines of existing objects. We note that this differs from other common applications in design, in which the objective is to construct new objects for given boundary conditions. We characterize the profile of Japanese handmade pantiles in Section 5.1, which is part of a joint work with T. Suzuki [13]; and we characterize keylines of a car's roof in Section 5.2, which is part of a joint work with K. T. Miura [14].

5.1 Keylines of Japanese handmade pantiles

Sangawara (Japanese pantiles) are the most common type of roof tiles in Japan and are thought to be unique to the country. Although the number of buildings with sangawara roofs is decreasing, landscapes with constructions having sangawara roofs are considered, by the community, to be one of the most beautiful and culturally Japanese scenes. Traditionally, sangawara were handmade from local clay by placing a clay plate on a wooden mold, beating it with a board called *tataki*, and stroking it with a board called *nadeita*. In recent times, they are mass-produced in limited areas, by metal mold presses. The mold shapes are thought to be based on the shape of the sangawara in the handmade era, but companies keep their designs a trade secret. We consider that it is important to characterize aesthetically pleasing curves like sangawara with mathematical formulas to be used in architectural design. Because of this, and the fact that the process involves bending the clay plate, we thought that the shape of sangawara could possibly be approximated by the Euler's elasticae. In Section 5.1.1, we explain how the handmade sangawara (simply referred to as pantiles) were collected, and how we

obtain the keyline of each pantile. In Section 5.1.2, we approximate those keylines to discrete Euler's elasticae.

5.1.1 Data collection and pre-processing

The pantiles that we measured were used in a house built around 1900 in Settsu city, Osaka prefecture. From the characteristic shapes of the pantiles, they were likely used from the original construction or replaced before the revision of the urban building law in 1924 after the Great Kanto Earthquake. According to the owners, most of the tiles were blown away when the 2nd Muroto Typhoon hit in 1961, so they were collected and re-roofed. After that, only a few of the pantiles were replaced before the house was demolished in March 2017. In a survey before the demolition, it was found that the roofs of this house were covered by four different sizes of pantiles that ranged from 240 to 280 mm in working width. Prior to dismantling the building, six rows of pantiles were preserved (A to F in Figure 5.1), covering those four sizes. We measured 37 pantiles of the C and F rows, with a working width of 270 mm (the most commonly used on this house), excluding the eave pantiles (C01, F01).

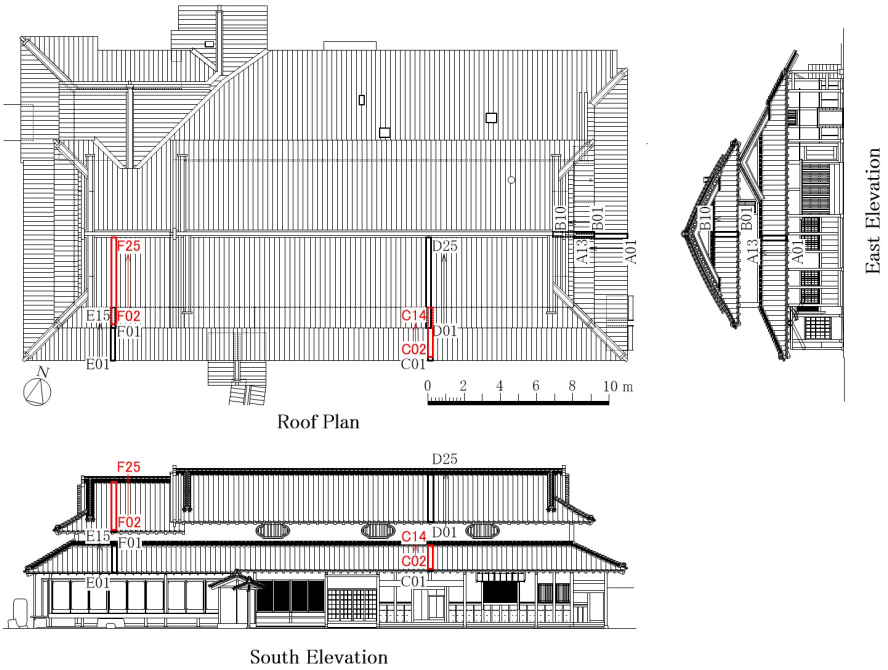

Figure 5.1: Preserved pantiles (black and red: A-F) and measured pantiles (red: C02-14, F02-25).

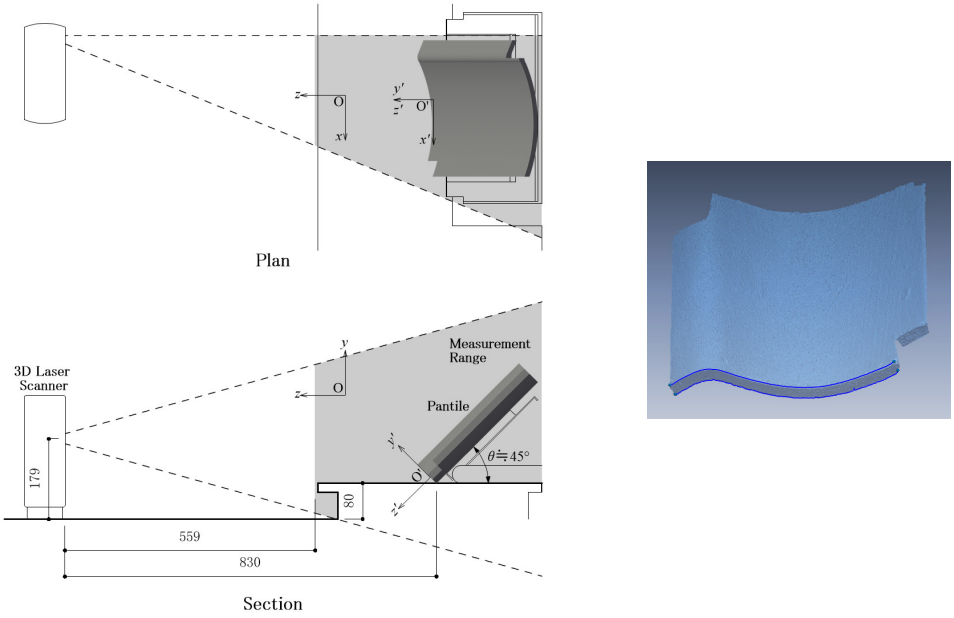

Figure 5.2: Left: Placement of 3D laser scanner and pantile during measurement. Right: Example of 3D keylines generated (C07).

The NextEngine's Ultra HD 3D laser scanner was used for the measurements, as shown in Figure 5.2. The mesh data obtained from the 3D laser scanner was read by 3D Systems' RapidWorks 64 4.1.0, a reverse modeling software. This software was used to synthesize and decimate its polygons finer than the scanner's measurement accuracy (0.3 mm) and then it automatically healed incorrect data and filled the holes in the meshes. The keylines used for this analysis correspond to the bottom front edge of the pantiles. Figure 5.2 shows an example of the keylines generated. By using the principal component analysis, the keylines were projected to a plane, and after processing these curves, we obtained discrete planar curves with constant step size. The keylines have one inflection point, and the curve is clearly asymmetric at this point. This makes difficult to formulate such curve in terms of a single elastica. Therefore, we estimate the inflection point of the curve, then we divide it in two segments and approximate each of them with different elasticae. We estimated the inflection point using a method inspired by the Ramer–Douglas–Peucker algorithm [8, 42], which was devised to *smoothen* a given discrete set of points by decimation.

5.1.2 Characterization by discrete Euler's elasticae

We considered the input curves to be 37 segments, corresponding to the segments of the keylines situated at the right-hand side of their estimated inflection points. To each segment, we applied the algorithm described in Section 3.3. From the parameters $\Theta = (x_0, y_0, h, \phi, z, q, k)$, the point $(x_0, y_0) \in \mathbb{R}^2$ was fixed at the inflection point, and the remaining five parameters were optimized. An example of the fairing is shown in Figure 5.3, the result after fairing all the curves is shown in Figure 5.4, and the resulting parameter values are summarized in Table 5.1.

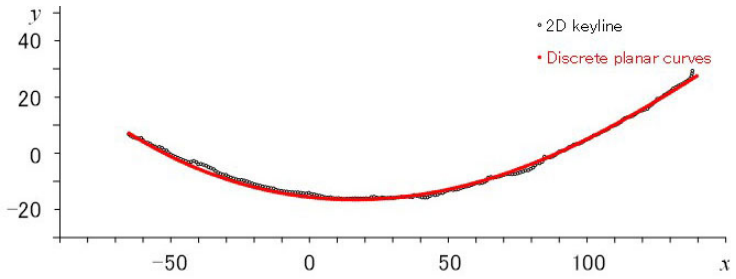

Figure 5.3: Example: fairing of the C07 lower keyline (black) to an Euler's elastica (red).

Lower keylines right (valley) side		h [mm]	ϕ [rad]	ϕ [grad]	z	q	k
C02–14, F02–15, 17–23, 25	mean	0.964	−0.168	−9.623	9.001×10^{-3}	5.919	0.353
	std. dev.	6.564×10^{-3}	2.078×10^{-3}	0.119	1.263×10^{-3}	1.789×10^{-3}	1.235×10^{-2}
F16		0.945	2.045	117.192	67.36	5.226	27.43
F24		1.007	2.478	141.986	121.8	28.28	27.39

Table 5.1: Calculation results for h, ϕ, z, q and k (mean and standard deviation). Because the values for F16 and F24 were noticeably different from the others, the means and standard deviations were calculated for the 35 keylines except for F16 and F24, and the values for F16 and F24 were written separately.

As Table 5.1 shows, there are 35 keylines (except for F16 and F24) that show very little variation in their parameters, and the discrete elasticae are similar in shape. The k values are close to 0.3, corresponding to the case with inflection points [WI]. The values of k for F16 and F24 are noticeably different, and correspond to the case without inflection point [NI]. We think that the variations in the parameters z and q, for the 35 elasticae [WI], are related to the estimation error of the inflection point. The effect that the local unevenness of the keylines, due to the

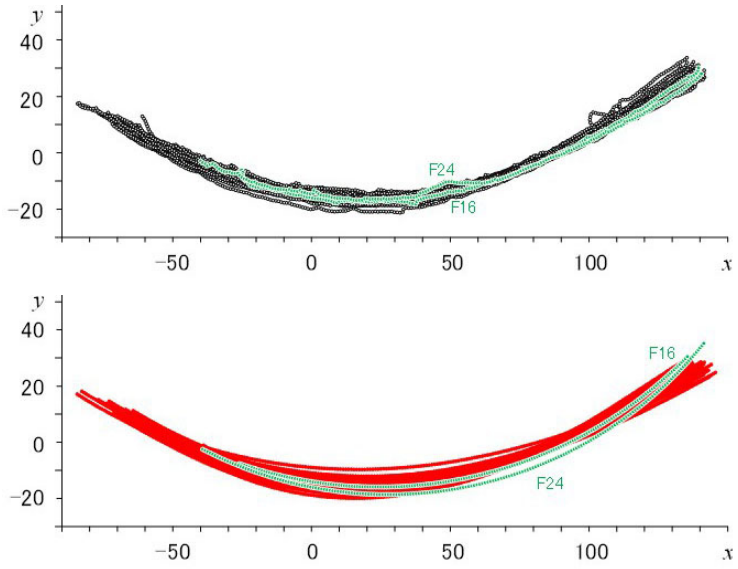

Figure 5.4: Upper: Input curves (black). Bottom: Approximating Euler's elastica (red). The highlighted curves (green) correspond to keylines that presented a statistically different result.

manufacturing and measuring process, has on the estimation of the inflection point should be examined. In conclusion, we found that 35 of the 37 lower keylines of the handmade pantiles could be approximated by discrete Euler's elasticae with a very small variation on the right-hand side of the inflection point. However, the errors of the estimated positions of the inflection points may affect the accuracy of the approximations.

5.2 Keylines of a car's roof

In order to test the fairing algorithm shown in Section 4.2 we characterize some simple profile lines of a car's roof (Toyota Prius). In Section 5.2.1 we explain how the keylines were collected and processed, and in Section 5.2.2 we approximate those keylines to log-aesthetic curves.

5.2.1 Data collection and pre-processing

A 3D model was obtained by measuring a scale model car with a 3D laser scanner (Hexagon 8330-7, measurement accuracy of 0.078 mm). This 3D model was stored in STL (Standard Triangle/Tessellation Language) format, which encodes

the geometry of the object in a triangular mesh. Using Rhinoceros 6, a computer-aided design software, we intercepted the 3D model with vertical planes, see Figure 5.5. Finally, we projected the curves into the plane and processed the discrete point to obtain a planar discrete curve with constant step size. The length of each curve is approximately 1500 mm, and the separation between each curve is 100 mm.

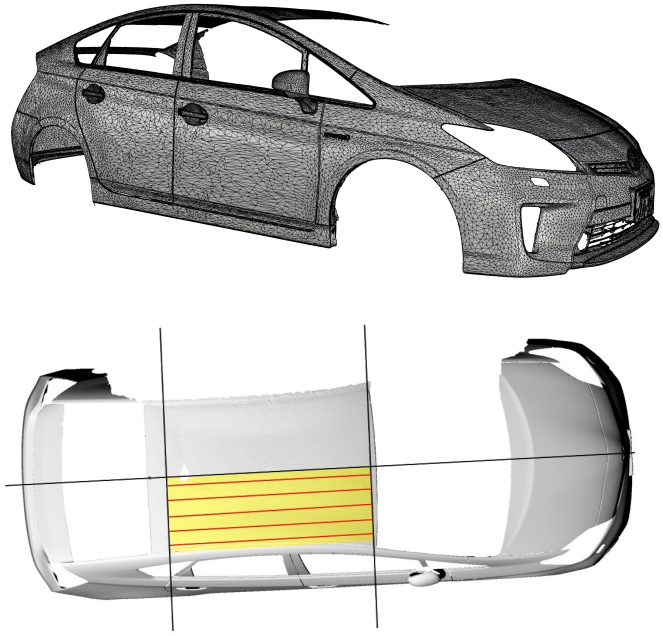

Figure 5.5: Top: 3D model (STL data). Bottom: Position of sampled curves, obtained from the interception of the 3D model and vertical planes (Software: Rhino 6). The black lines represent the intercepting planes, and the red lines, in the highlighted area, represent the resulting curves. From the center to the bottom, curves are labelled as ps_1, ps_2, ps_3, ps_4 and ps_5.

We observed that the curvature of the keylines is highly irregular, as a product of the measuring technique employed. To reduce the noise, we proceeded as follows: Let the curve $\gamma_n \in \mathbb{R}^2$, $n = 0, \ldots, N-1$ with a constant step size $h > 0$, be the raw data; then:

(0) — Let $\check{N} = 3$.

(1) — For $\check{N} < N$, apply the Ramer–Douglas–Peucker algorithm to γ_n, to obtain a new curve $\check{\gamma}_n$, $n = 0, \ldots, \check{N}-1$, such that $\check{\gamma}_0 = \gamma_0$ and $\check{\gamma}_{\check{N}-1} = \gamma_{N-1}$.

(2) — Construct a cubic spline curve $\gamma_{cs}(t)$, $t \in [0, L]$, using $\check{\gamma}_n$, $n = 0, \ldots, \check{N} - 1$, as the control points; hence, $\gamma_{cs}(0) = \gamma_0$ and $\gamma_{cs}(L) = \gamma_{N-1}$.

(3) — Construct a discrete curve $\bar{\gamma}_n$, $n = 0, \ldots, N-1$ with step size h, by sampling the cubic spline $\gamma_{cs}(t_n)$ in a appropriate manner such that $\|\gamma_{cs}(t_{n+1}) - \gamma_{cs}(t_n)\| = h$ and $\bar{\gamma}_n = \gamma_{cs}(t_n)$, $n = 0, \ldots, \check{N} - 1$.

(4) — If the residual R is greater than a prescribed error η,

$$R = \frac{1}{L^2} \sum_{n=0}^{N-1} \|\bar{\gamma}_n - \gamma_n\| h > \eta, \tag{5.1}$$

repeat from step (1), with a greater value of $\check{N}$. Otherwise, the process ends.

In our case, we used $\eta = 10^{-3}$, and we observed that this produces a smoother plot for the curvature, see Figure 5.6. Hence, we use $\bar{\gamma}_n$, instead of γ_n, as the input curve of the fairing process.

5.2.2 Characterization by log-aesthetic curves

We applied the algorithm described in Section 4.2 to the 5 curves obtained from the previous analysis. We noticed that the admissible set U for the parameters Θ, as defined in (4.40), was too broad and unexpected jumps in the value of the parameters produced unrealistic outputs. To keep the optimization relatively close to the initial guess, we decided to constrain the admissible set to $\bar{U}_{0.1}$, defined by

$$\bar{U}_{0.1} := U \cap \left\{\Theta \in \mathbb{R}^7 : \left|\Theta_i - \bar{\Theta}_i\right| < 0.1\bar{\Theta}_i\right\}, \tag{5.2}$$

where $\bar{\Theta}$ is the initial guess for the IPOPT method, as described in Section 4.2.2. In this way, $\bar{U}_{0.1}$ constrain the final result to be in a 10% range of the initial guess. Final results are presented in Figure 5.7. We note that the parameters that we obtained provide a good fit of the input curve. We can observe that, despite the curves being similar in shape to each other, the values of the parameter α have big variations. However, the final result is still a good fit, after finding the remaining parameters. Let us note that, this algorithm allows us to input the parameter α by hand (or by replacing (4.55) by an alternative expression or algorithm) and then we can continue with the next steps without any further change. In particular, in Figure 5.8 we show the results of the initial guess obtained by fixing $\alpha = 2$. The fact that we still obtained a good fit is attributed to the input curve having a *soft* varying curvature. We conclude that the method proposed has a good performance, however further analysis on the recovery of the parameter α is required.

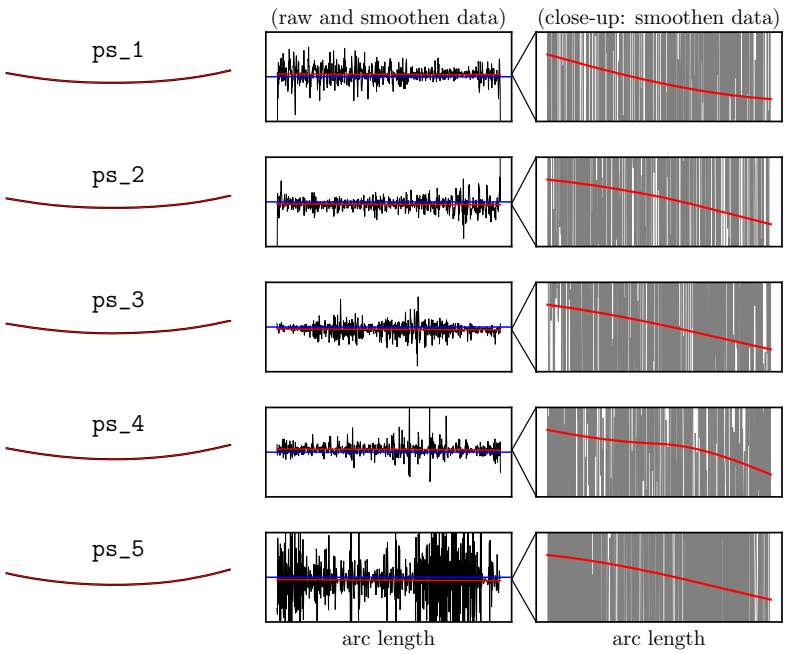

Figure 5.6: Input curves without smoothing. Left column: Each curve represent a different section of the car's roof. Black lines are raw data and red lines are the smoothen data (the input curves after noise reduction). Left column: raw and smoothen curves in the plane, practically overlapping with each other. Middle column: Curvature plot vs arc length for their corresponding input curves, where the blue line is a reference for the constant $\kappa = 0$. Right column: same as middle column, with a close-up on the smoothen data.

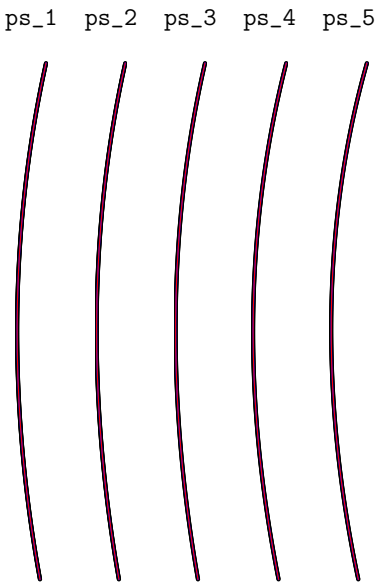

	1	2	3	4	5
alpha	4.44	1.73	0.30	-4.66	0.62
S	3070.37	2885.32	4125.71	3597.87	4966.19
s0	0.10	0.11	-0.27	-0.31	-0.55
l	0.49	0.52	0.37	0.42	0.31
phi	-1.89	-1.90	-1.49	-1.48	-1.08
x0	-552.73	-549.88	-544.74	-537.90	-529.70
y0	3346.76	3346.06	3346.39	3347.03	3349.25

Figure 5.7: Discrete curves approximated by LAC. Each curve represent a different section of half of the car roof, taken at 100 mm apart. Black lines: input curves. Red lines: LAC output. The parameters in the table correspond to the smooth LAC, according to Proposition 4.4, recovered from the approximation defined in (4.34) using (4.33)

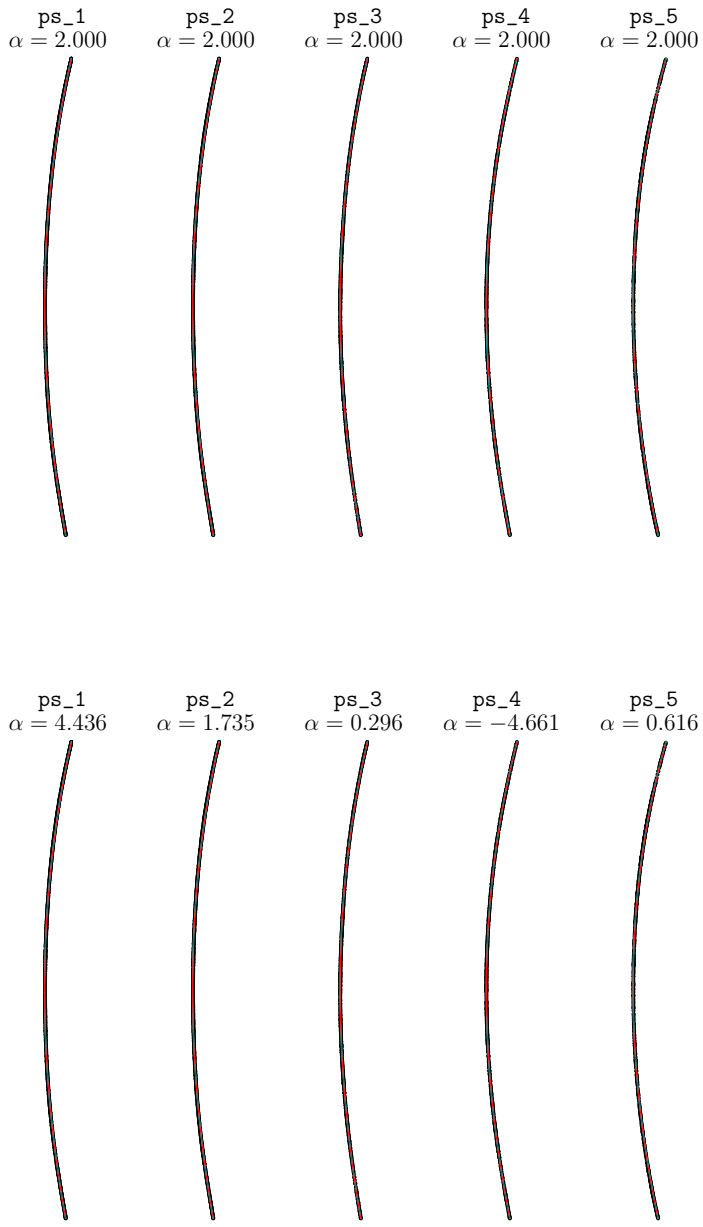

Figure 5.8: Initial guess, with fixed $\alpha = 2$ at the top, and fixed by the algorithm (Equation (4.55)) at the bottom. Black lines: Input curves. Red lines: LAC Initial guess.

Chapter 6

Conclusions

Regarding the discrete Euler's elastica, we provided a review of the literature on the integrable discretization and showed concrete parameterizations that recover the continuous framework. Although several results are well-known facts, explicit expressions and proof are not found in the literature. In particular, we showed that there are two possible definitions for the discrete Euler's elastica which are, indeed, equivalent (Proposition 3.12). We showed that their explicit solutions can be written in terms of the Jacobi elliptic functions, and could be checked by simply using the addition formulas for the Jacobi elliptic functions. In Section 3.3, we presented an algorithmic approach to reconstruct a discrete Euler's elastica by seven parameters. This work can be seen as an extension of the algorithm provided by D. Brander et al. in [6], and it can be used in cases where the input curve is intrinsically discrete. We used our algorithm in Section 5.1 to the problem of characterizing the profile keylines of Japanese handmade pantiles.

Regarding the log-aesthetic curve, we have shown in Proposition 4.4 that any LAC segment (with parameter $\alpha \neq 1$) can be obtained from a *basic* LAC by applying similarity transformations. This shows that the family of LAC with the same parameter α is self-similar. In recent studies [20], the similarity geometry framework was used to provide a similarity geometry analogue of the *elastic energy* and to construct more general LAC and discrete LAC. We consider that further studies exploiting the self-similarity properties of the LAC will be crucial to attain generalized aesthetic surfaces and space curves. In Section 4.2, we used Proposition 4.4 to construct an algorithmic approach to recover the seven parameters that uniquely identify a given LAC, proceeding in a similar manner than for the Euler's elastica case. We expect that this algorithm will be used as a new tool to characterize an existing object, which is particularly useful in reverse engineering. Moreover, because the LAC is regarded as an aesthetically pleasing shape, there exists an increasing interest from the industry to have algorithms

like the ones presented that can be used in computer-aided design softwares. In this thesis, and as a simple example of usage, in Section 5.2 we characterized the profile lines of a car's roof. As it was first discussed by T. Harada et al. in [15], they considered that the value of the parameter α gives specific attributes to the curve's character. However, we have seen that curves that are similar can possibly have different values of α, which is a consequence of the curves not having several changes in magnitude for their curvatures. One possible way to solve this problem is by allowing the designer to input the expected value of α. Finally, further extensions to this method could be the generalization into space curves, or aesthetic surfaces, for which a result similar to Proposition 4.4 is needed. We think that investigating generalizations that use the self-similar properties is a first step to approach this task.

Bibliography

[1] T. Banchoff and S. Lovett, Differential geometry of curves and surfaces, 2nd ed., CRC Press, New York (2015)

[2] J. Berkmann and T. Caelli, Computation of surface geometry and segmentation using covariance techniques, IEEE Trans Pattern Anal Mach Intell **16**(11), 1114–1116 (1994)

[3] A. Bobenko, Geometry II – discrete differential geometry, lecture notes available at
`https://page.math.tu-berlin.de/~bobenko/Lehre/Skripte/DDG07.pdf`
(May 31, 2007)

[4] A. Bobenko and U. Pinkall, Discrete surface with constant negative Gaussian curvature and the Hirota equation, J. Differential Geom. **43**, 527–611 (1996)

[5] A. I. Bobenko and Yu. B. Suris, Discrete time Lagrangian mechanics on lie groups, with an application to the Lagrange top, Commun. Math. Phys. **204**, 147–188 (1999)

[6] D. Brander, J. Gravesen and T.B. Nørjerg, Approximation by planer elastic curves, Adv. Comput. Math. **43**, 25–43 (2017)

[7] M. P. Do Carmo, Differential geometry of curves and surfaces: revised and updated second edition, Dover Publications, New York (2016)

[8] D. Douglas and T. Peucker, Algorithms for the reduction of the number of points required to represent a digitized line or its caricature, The Canadian Cartographer **10**(2), 112-–122 (1973)

[9] J. Fernández, S. E. Graiff Zurita and S. Grillo, Error analysis of forced discrete mechanical systems, J. Geom. Mech. **13**(4), 533–606 (2021)

[10] R. U. Gobithaasan and K. T. Miura, Aesthetic spiral for design, Sains Malaysiana **40**, 1301–1305 (2011)

[11] R. U. Gobithaasan, Y. Siew Wei and K. T. Miura, Log-aesthetic curves for shape completion problem, J. Appl. Math. **2014**, 960302 (2014)

[12] R. E. Goldstein and D.M. Petrich, The Korteweg-de Vries hierarchy as dynamics of closed curves in the plane, Phys. Rev. Lett. **67**, 3203–3206 (1991)

[13] S. E. Graiff Zurita, K. Kajiwara and T. Suzuki, Fairing of discrete planar curves by integrable discrete analogue of Euler's elasticae, preprint, arXiv:2111.00804 [nlin.SI] (2021)

[14] S. E. Graiff Zurita, K. Kajiwara and K. T. Miura, Fairing of planar curves to log-aesthetic curves, preprint, arXiv:2206.00235 [math.NA] (2022)

[15] T. Harada, N. Mori and K. Sugiyama, Study of quantitative analysis of curve's character, Bull. JSSD **40**, 9–16 (1994) (in Japanese)

[16] R. Hirota, Nonlinear partial difference equations. III. Discrete sine-Gordon equation, J. Phys. Soc. Jpn. **43**, 2079–2086 (1977)

[17] R. Hirota, Discretization of the potential modified KdV equation, J. Phys. Soc. Jpn. **67**, 2234–2236 (1998)

[18] T. Hoffmann, Discrete differential geometry of curves and surfaces, MI Lecture Notes **18**, Kyushu University, Fukuoka (2009)

[19] T. Hoffmann and N. Kutz, Discrete curves in $\mathbb{C}\mathrm{P}^1$ and the Toda lattice, Stud. in Appl. Math. **113**, 31–55 (2004)

[20] J. Inoguchi, Y. Jikumaru, K. Kajiwara, K. T. Miura and W. K. Schief, Log-aesthetic curves: similarity geometry, integrable discretization and variational principles, preprint, arXiv:1808.03104v2 [nlin.SI] (2021)

[21] J. Inoguchi, K. Kajiwara, N. Matsuura and Y. Ohta, Motion and Bäcklund transformations of discrete planar curves, Kyushu J. Math. **66**, 303–324 (2012)

[22] J. Inoguchi, K. Kajiwara, N. Matsuura and Y. Ohta, Discrete mKdV and discrete sine-Gordon flows on discrete space curves, J. Phys. A: Math. Theoret. **47**, 235202 (2014)

[23] J. Inoguchi, K. Kajiwara, K. T. Miura, M. Sato, W. K. Schief and Y. Shimizu, Log-aesthetic curves as similarity geometric analogue of Euler's elasticae, Comput. Aided Geom. Des. **61**, 1–5 (2018)

[24] K. Kajiwara, M. Noumi and Y. Yamada, Geometric aspects of Painlevé equations, J. Phys. A: Math. Theor. **50**(7), 073001 (2017)

[25] K. Kajiwara, Y. Ohta, J. Satsuma, B. Grammaticos and A. Ramani, Casorati determinant solutions for the discrete Painlevé-II equation, J. Phys. A: Math. Gen. **27**(3), 915–922 (1994)

[26] L. D. Landau and E. M. Lifshitz, Theory of elasticity, Course of theoretical physics, vol. 7, Pergamon Press, London (1959)

[27] D. F. Lawden, Elliptic functions and applications, Applied Mathematical Sciences, vol. 80, Springer-Verlag, New York (1989)

[28] R. Levien, The Elastica: a mathematical history, EECS Department, University of California, Berkeley, UCB/EECS-2008-103 (2008)

[29] R. Levien and C.H. Séquin, Interpolating splines: which is the fairest of them all? Comput. Aided Des. Appl. **6**, 91–102 (2009)

[30] J. E. Marsden and M. West, Discrete mechanics and variational integrators, Acta Numererica **10**, 357–514 (2001)

[31] S. Matsutani, Euler's elastica and beyond, J. Geom. Symmetry Phys. **17**, 45–86 (2010)

[32] N. Matsuura, Discrete KdV and discrete modified KdV equations arising from motions of planar discrete curves, Int. Math. Res. Notices **2012**(8), 1681–1698 (2012)

[33] N. Matsuura, An explicit formula for discrete planar elastic curves, talk given at the Annual Meeting of Mathematical Society of Japan (March 18, 2020) (in Japanese)

[34] E. M. McMillan, Some thoughts on stability in nonlinear periodic focusing systems, Lawrence Berkeley National Laboratory (1967)

[35] K. T. Miura and R. U. Gobithaasan, Aesthetic design with log-aesthetic curves and surfaces, in: Mathematical Progress in Expressive Image Synthesis III, eds. by Y. Dobashi and H. Ochiai, Mathematics for Industry **24**, 107–120. Springer, Singapore (2015)

[36] K. T. Miura, J. Sone, A. Yamashita and T. Kaneko, Derivation of a general formula of aesthetic curves, in: proceedings of the Eighth International Conference on Humans and Computers (HC2005), 166–171 (2005)

[37] D. Mumford, Elastica and computer vision, in: Algebraic Geometry and Its Applications, 491–506. Springer, New York (1994)

[38] NIST Digital Library of Mathematical Functions, `https://dlmf.nist.gov/`

[39] G. W. Patrick and C. Cuell, Error analysis of variational integrators of unconstrained Lagrangian systems, Numer. Math. **113**, 243—264 (2009)

[40] G. R. W. Quispel, J. A. G. Roberts and C.J. Thompson, Integrable mappings and soliton equations, Phys. Lett. **A126**, 419–421 (1988)

[41] A. Ramani, B. Grammaticos and J. Hietarinta, Discrete versions of the Painlevé equations, Phys. Rev. Lett. **67**, 1829–1832 (1991)

[42] U. Ramer, An iterative procedure for the polygonal approximation of plane curves, Comput. Graph. Image Process. **1**, 244–256 (1972)

[43] D. A. Singer, Lectures on elastic curves and rods, in: Curvature and variational modeling in physics and biophysics, AIP Conf. Proc. **1002**, 3–32 (2008)

[44] K. Sogo, Variational discretization of Euler's elastica problem, J. Phys. Soc. Jpn. **75**, 064007 (2006)

[45] D. Takahashi, T. Tokihiro, B. Grammaticos, Y. Ohta and A. Ramani, Constructing solutions to the ultradiscrete Painlevé equations J. Phys. A: Math. Gen. **30**, 7953–7966 (1997)

[46] M. Toda, Introduction to elliptic functions (Japanese book), Nippon Hyoronsha, Tokyo (2001)

[47] A. Wächter and L.T. Biegler, On the implementation of an interior-point filter line-search algorithm for large-scale nonlinear programming, Math. Program., Ser. A **106**, 25–57 (2006)

[48] E. T. Whittaker and G. N. Watson, A course of modern analysis, 3rd ed., Cambridge University Press, London (1920)

[49] R. C. Yates, A handbook on curves and their properties, Edwards Brothers Inc., Michigan (1947)

[50] N. Yoshida and T. Saito, Interactive aesthetic curve segments, Visual Comput **22**, 896—905 (2006)

[51] R. Ziatdinov, N. Yoshida and T. Kim, Analytic parametric equations of log-aesthetic curves in terms of incomplete gamma functions, Comput. Aided Geom. Des. **29**(2), 129–140 (2012)